Chemogenetic sensory fMRI reveals behaviorally relevant bidirectional changes in primate somatosensory network

AUTHOR(S):

Hirabayashi, Toshiyuki; Nagai, Yuji; Hori, Yukiko; Inoue, Ken-ichi; Aoki, Ichio; Takada, Masahiko; Suhara, Tetsuya; Higuchi, Makoto; Minamimoto, Takafumi

CITATION:

Hirabayashi, Toshiyuki ...[et al]. Chemogenetic sensory fMRI reveals behaviorally relevant bidirectional changes in primate somatosensory network. Neuron 2021, 109(20): 3312-3322

ISSUE DATE:

2021-10

URL:

http://hdl.handle.net/2433/265516

Neuron

Article

Chemogenetic sensory fMRI reveals behaviorally relevant bidirectional changes in primate somatosensory network

Highlights

- FMRI-guided chemogenetic silencing of macaque SI hand region induced grasping deficit
- Sensory-evoked BOLD response decreased at local and remote areas in grasping network
- Hand region silencing enhanced foot representation with behavioral hypersensitization
- Chemogenetic fMRI revealed behaviorally relevant bidirectional network modulation

Authors

Toshiyuki Hirabayashi, Yuji Nagai, Yukiko Hori, ..., Tetsuya Suhara, Makoto Higuchi, Takafumi Minamimoto

Correspondence

hirabayashi.toshiyuki@qst.go.jp

In brief

Hirabayashi et al. demonstrate that chemogenetic silencing of macaque SI hand representation impairs grasping and enhances sensitivity to foot stimulation. These behavioral effects co-occur with decreased fMRI activation in the grasping-related network and enhanced foot representation. This study reveals how local inactivation affects the network operation within and across areas.

Hirabayashi et al., 2021, Neuron *109*, 3312–3322
October 20, 2021
https://doi.org/10.1016/j.neuron.2021.08.032

CellPress

CellPress OPEN ACCESS

Neuron

Article

Chemogenetic sensory fMRI reveals behaviorally relevant bidirectional changes in primate somatosensory network

Toshiyuki Hirabayashi,[1,5,*] Yuji Nagai,[1] Yukiko Hori,[1] Ken-ichi Inoue,[2,3] Ichio Aoki,[4] Masahiko Takada,[2] Tetsuya Suhara,[1] Makoto Higuchi,[1] and Takafumi Minamimoto[1]

[1]Department of Functional Brain Imaging, National Institutes for Quantum and Radiological Sciences and Technology, Anagawa 4-9-1, Inage-ku, Chiba, Japan
[2]Systems Neuroscience Section, Primate Research Institute, Kyoto University, Inuyama, Aichi 484-8506, Japan
[3]PRESTO, Japan Science and Technology Agency, Kawaguchi, Saitama, Japan
[4]Department of Molecular Imaging and Theranostics, National Institutes for Quantum and Radiological Sciences and Technology, Anagawa 4-9-1, Inage-ku, Chiba, Japan
[5]Lead contact
*Correspondence: hirabayashi.toshiyuki@qst.go.jp
https://doi.org/10.1016/j.neuron.2021.08.032

SUMMARY

Concurrent genetic neuromodulation and functional magnetic resonance imaging (fMRI) in primates has provided a valuable opportunity to assess the modified brain-wide operation in the resting state. However, its application to link the network operation with behavior still remains challenging. Here, we combined chemogenetic silencing of the primary somatosensory cortex (SI) with tactile fMRI and related behaviors in macaques. Focal chemogenetic silencing of functionally identified SI hand region impaired grasping behavior. The same silencing also attenuated hand stimulation-evoked fMRI signal at both the local silencing site and the anatomically and/or functionally connected downstream grasping network, suggesting altered network operation underlying the induced behavioral impairment. Furthermore, the hand region silencing unexpectedly disinhibited foot representation with accompanying behavioral hypersensitization. These results demonstrate that focal chemogenetic silencing with sensory fMRI in macaques unveils bidirectional network changes to generate multifaceted behavioral impairments, thereby opening a pivotal window toward elucidating the causal network operation underpinning higher brain functions in primates.

INTRODUCTION

The functional magnetic resonance imaging (fMRI) has been widely used to examine brain-wide network operation underlying a variety of cognitive, affective, and motor functions in non-human primates, providing opportunities for a profound understanding of the corresponding functions in humans in health and disease (Vanduffel et al., 2014). Combining neuromodulation including electrical stimulation or muscimol injection with the monkey fMRI has shown to be a powerful approach for causally linking neural activity to behavior or testing neural coupling across brain regions (Bogadhi et al., 2019; Ekstrom et al., 2008; Klink et al., 2021; Miyamoto et al., 2017; Moeller et al., 2008; Rocchi et al., 2021; Schmid et al., 2010; Tolias et al., 2005; Van Dromme et al., 2016; Verhagen et al., 2019; Wilke et al., 2012; Xu et al., 2019; Yang et al., 2018). Compared with conventional neuromodulation approaches, genetic intervention has certain advantages, including anatomical and/or cell-type specificity of the manipulation target, which has been applied to non-human primates to change behavior and/or local neuronal activity at the manipulated region (Deffains et al., 2021; El-Shamayleh and Horwitz, 2019; Eldridge et al., 2016; Nagai et al., 2016; Raper et al., 2019; Upright et al., 2018). Given that the impact of focal neuromodulation is not necessarily localized to the manipulation target but extends to anatomically and/or functionally connected remote regions, induced behavioral changes would reflect the altered network operation (Bergmann and Hartwigsen, 2021; Carrera and Tononi, 2014). A few recent studies in non-human primates have shown the effect of genetic neuromodulation on the fMRI signal (Gerits et al., 2012; Grayson et al., 2016; Ohayon et al., 2013; Vancraeyenest et al., 2020). However, all those studies were conducted in the resting state, and thus whether and how genetic neuromodulation affects task- or sensory-evoked network fMRI signal to change behavior has not been examined. Although the network effect of focal manipulation is largely predictable from anatomical connections in the resting state (Grayson et al., 2016), it would be more complicated when the perturbation interacts with task- or sensory-evoked activity. Indeed, the impact of neuromodulation drastically differs depending on the brain state (Bestmann et al., 2008; Blankenburg et al., 2008; Davare et al., 2010; Ekstrom et al., 2008; Silvanto et al., 2008; Yang et al., 2021).

Such a difference becomes more critical in silencing because the effects would be obscured in the resting state without explicit brain activity to be suppressed (Davare et al., 2010). Moreover, considering the difficulty in applying genetic neuromodulation to primates (Galvan et al., 2018; Tremblay et al., 2020), it would not be trivial whether and how genetic silencing affects robustly evoked blood-oxygenation-level-dependent (BOLD) signal in primates, which would be a pivotal step toward elucidating the causal network operation underlying higher brain functions in primates.

Furthermore, the effect of silencing at remote regions would not necessarily be deactivation because silencing of a given network node can result in disinhibition of another node (Blankenburg et al., 2008), where such between-node relationships would be difficult to predict only from their anatomical connectivity. Mutually inhibitory nodes are ubiquitous in the brain including lateral inhibition in the sensory cortices (Chernov et al., 2018; Shmuel et al., 2006; Tal et al., 2017). Such neuromodulation-induced unpredictable bidirectional changes in network activity could be unveiled via concurrent neuromodulation and fMRI. This provides a profound understanding of the complex interactive operation of the brain network, which would predict a previously overlooked behavioral impact as well.

To address these issues, we examined the effects of fMRI-guided chemogenetic silencing on both sensory-evoked network operation and its relevant behaviors in macaques. We identified the hand index finger (D2) region of the primary somatosensory cortex (SI_{D2}) via somatosensory fMRI and focally injected adeno-associated virus (AAV) vector encoding an inhibitory designer receptor exclusively activated by designer drug (inhibitory DREADD, hM4Di) (Roth, 2016). Administration of recently developed, highly selective and stable DREADD actuator (Nagai et al., 2020) specifically impaired fine grasping behavior with the contralateral D2 and attenuated hand D2-mediated sensory-evoked BOLD signal at both SI_{D2} and the grasping-related downstream network. The same manipulation further induced unexpected disinhibition of a distant body part representation, which resulted in behavioral hypersensitization. Together, these results demonstrate that focal chemogenetic silencing concurrent with sensory fMRI unveils bidirectional changes in the network operation underlying the induced multifaceted behavioral impairments in macaques.

RESULTS

In order to functionally identify SI_{D2} as the target of focal chemogenetic silencing, we measured BOLD signal in response to sensory stimulation using 7T-MRI under light sedation with propofol (Figures 1A and S1A–S1C; STAR Methods). Consistent with previous studies (Arcaro et al., 2019; Chen et al., 2007; Cléry et al., 2020; Dutta et al., 2014; Hayashi et al., 1999; Lipton et al., 2006; Nagasaka et al., 2020; Sharma et al., 2018; Wang et al., 2013), cutaneous tactile stimulation of hand D2 evoked a significant BOLD response at the contralateral SI ($p < 0.05$, FWE-corrected) (Figure 1B; STAR Methods). We then injected an AAV vector for the neuron-specific expression of inhibitory DREADD (hM4Di) with GFP as a marker protein into the identified SI_{D2} (Figure 1A). To precisely inject the virus vector into SI_{D2}, we prepared a 3D printed brain model constructed from computed tomography (CT) images of the skull on which MR images of the brain structure and coregistered SI_{D2} activation map were overlaid. We mounted the brain model on the stereotaxic frame and determined injection coordinates of four points with 1- to 1.5-mm intervals that approximately spanned the identified SI_{D2} (Figure S1D; STAR Methods). Seven weeks after the injection, DREADD expression was visualized via *in vivo* positron emission tomography (PET) imaging with a DREADD-selective probe ^{11}C-labeled deschloroclozapine (DCZ) (Nagai et al., 2020). The results revealed prominent DREADD expression at the virus vector-injected region (Figures 1C and S1F), which overlapped with SI_{D2} (Figures 1B and 1C). The results were consistent between two monkeys that received DREADD transduction (Figures S1E and S1F). Consistent with a previous study (Nagai et al., 2020), postmortem immunohistochemical analysis verified the PET results (Figure 1D).

Previous studies in both humans and macaques have suggested that intact somatosensory processing is essential for grasping behavior with the contralateral hand (Brochier et al., 1999; Hikosaka et al., 1985; Jeannerod et al., 1984; Thompson et al., 2017). To examine the behavioral impact of DREADD-induced focal SI_{D2} silencing, we thus trained the two monkeys to perform a modified Brinkman board task (Brinkman, 1984; Brinkman and Kuypers, 1973; Rouiller et al., 1998). Briefly, a plastic board with rectangular slots was placed in front of a monkey chair. Monkeys picked up small food pellets from the slots using D1 (thumb) and D2 of either the contralateral or ipsilateral hand (precision grip) (Nishimura et al., 2007; Sawada et al., 2015) to the DREADD-expressing SI_{D2} (Figure 2A). The time duration for correctly picking up all the pellets was measured as an index of manual dexterity using hand D2. Systemic administration of the highly selective, potent, and metabolically stable DREADD agonist DCZ (Nagai et al., 2020) significantly prolonged the duration in the contralateral hand condition ($p < 0.004$ for each of two monkeys, paired t test) (Figure 2B, red), suggesting deteriorated fine-grasping behavior. By contrast, the task performance in the ipsilateral hand condition was not significantly affected by DCZ administration in the same experimental sessions in either monkey ($p > 0.1$) (Figure 2B, blue), leading to a significant difference in the DCZ-induced performance change between the contralateral and ipsilateral hand conditions in the two monkeys ($p < 0.002$, paired t test) (Figure 2B, blue versus red). These results suggest that the effect of DCZ was specific to the hemisphere into which the DREADD was transduced and thus was not due to a side effect such as off-target action to endogenous receptors (Eldridge et al., 2016; Nagai et al., 2020; Upright and Baxter, 2020) (see Discussion). DCZ administration did not significantly affect the number of correctly picked objects for either the ipsilateral or contralateral hand in either monkey ($p > 0.05$, paired t test) (Figure S2A). In order to assess the specificity of the observed behavioral impairment more closely, we also examined the performance of coarse grasping of larger objects placed on a flat plate (Figure S2B). This task similarly required hand reaching, but the grasping was performed with the whole hand (Figure S2B, left), and manual dexterity was only minimally required. In contrast to the fine grasping task, performance of the coarse grasping with the contralateral hand did not

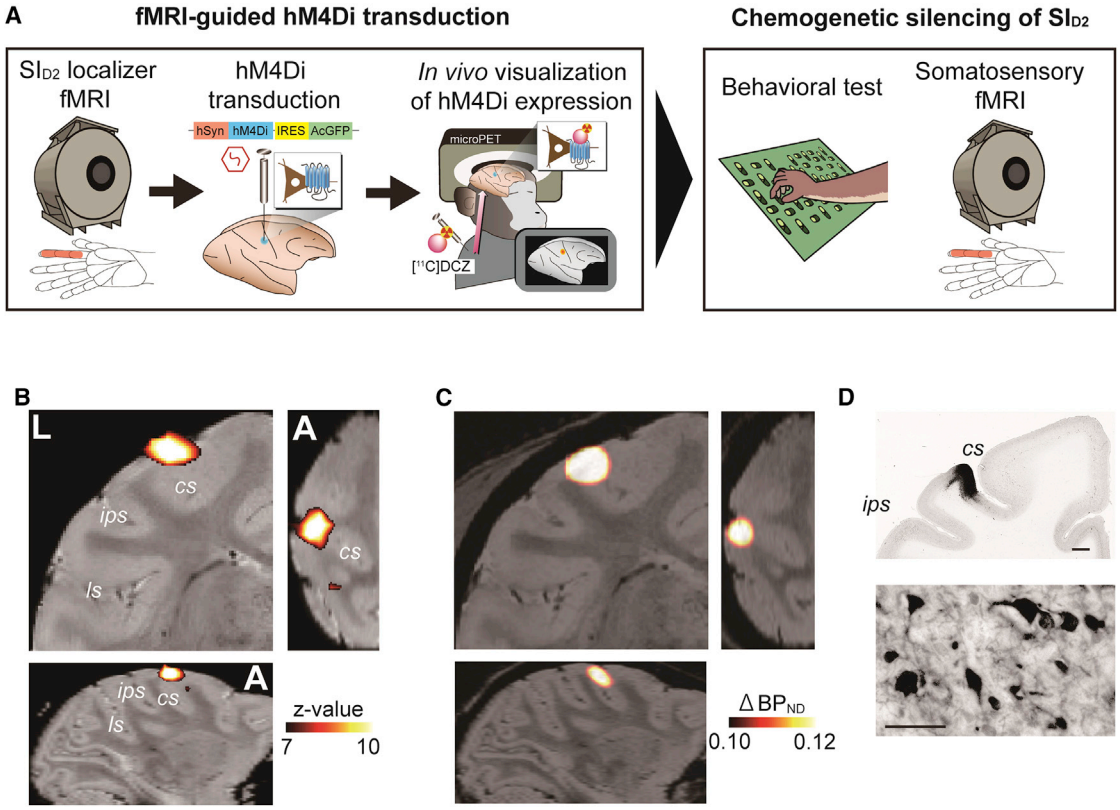

Figure 1. FMRI-guided transduction of hM4Di into the macaque SI$_{D2}$

(A) Experimental design and procedure.

(B) BOLD response in the SI of monkey 1 to cutaneous right hand stimulation for targeting hM4Di transduction. Right and bottom: axial and sagittal slices, respectively. cs, central sulcus; ips, intraparietal sulcus; ls, lateral sulcus; L, left; A, anterior.

(C) *In vivo* [^{11}C]DCZ PET image of hM4Di expression at the viral vector injection site in monkey 1.

(D) Histologically verified expression of co-transduced GFP at the viral vector injection site in monkey 1. Bottom: magnified view of the top panel, showing single neurons expressing GFP. Scale bar, 2 mm (top) and 50 μm (bottom).

See also Figure S1.

significantly change following DCZ administration with the same dose (monkey 2, $p > 0.4$, paired t test) (Figure S2B, right), suggesting that the observed behavioral impairment was specific to precision grasping, for which intact D2 representation would be essential. These results demonstrate that fMRI-guided focal chemogenetic silencing of SI$_{D2}$ exerted an impact specifically on fine grasping behavior with the contralateral hand D2 in macaques.

To assess whether and how the DREADD-induced, behaviorally effective SI$_{D2}$ silencing affects the relevant fMRI signal, we next conducted somatosensory-evoked fMRI concurrent with the same SI$_{D2}$ silencing. First, we confirmed that significant and robust BOLD activity of the DREADD-expressing SI$_{D2}$ was elicited by cutaneous tactile stimulation of the contralateral hand D2 in the control condition with systemic vehicle administration ($p < 0.05$, FWE-corrected) (Figure 3A, left top). The result indicates the intact function of SI$_{D2}$ following the virus vector injection and DREADD expression, at least in generating sensory-evoked BOLD signal. As a result of systemic DCZ administration, SI$_{D2}$ activation evoked by the same sensory stimulation was largely attenuated in the DREADD-expressing hemisphere (Figure 3A, left middle), leading to a significantly reduced activity compared to the vehicle control condition (vehicle versus DCZ, $p < 0.001$, uncorrected) (Figure 3A, left bottom). A region of interest (ROI) analysis revealed consistency and stability of the results from the following three different points of view. First, DCZ-induced reduction of the sensory-evoked BOLD signal in the contralateral SI$_{D2}$ was consistently observed in both monkeys ($p < 0.001$, unpaired t test) (Figure 3B, left). Second, in the paired alternation design of scanning sessions with vehicle/DCZ administration (STAR Methods), signal reduction in the DCZ session compared with the previous vehicle session was consistently observed across different pairs of successive sessions in both monkeys (Figure S3, left). Third, consistent with the reported time course of the silencing effect of DCZ *in vivo* (Nagai et al., 2020), DCZ-induced BOLD signal reduction was significant from the first run (18 min long) in a scanning session, which started 10 min following systemic intravenous DCZ administration, and remained stable across repeated runs within a session lasting for ~2 h (Figure S3, right; STAR Methods). In contrast to the DREADD-expressing hemisphere, SI$_{D2}$ activity in the intact hemisphere via contralateral D2 stimulation in the

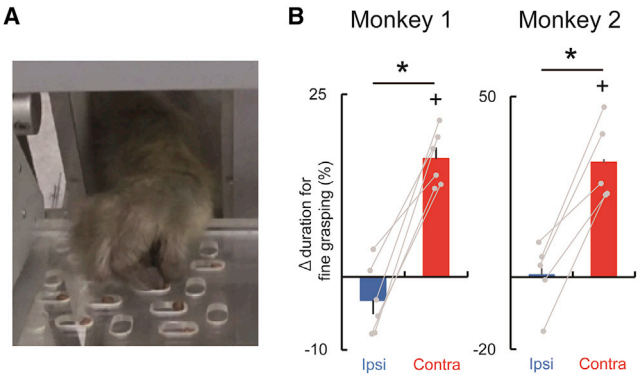

Figure 2. Behavioral impact of DREADD-induced SI_{D2} silencing

(A) Modified Brinkman board task for testing the performance of fine grasping with each hand. Monkeys used thumb and index fingers to pick up small food pellets.

(B) Task performance of each monkey. Positive values represent delayed task performance following DCZ administration. Ipsi and contra depict ipsilateral and contralateral hand to the DREADD-expressing SI_{D2}, respectively. Gray line depicts the performance in each session. Error bars, SEM. *$p < 0.002$, paired t test. +$p < 0.004$, paired t test for difference between pre- and post-administration of DCZ, corrected for multiple comparisons.

See also Figure S2.

same scanning session was not significantly different between vehicle and DCZ conditions in either monkey ($p > 0.4$) (Figures 3A and 3B, right). This interhemispheric difference in the effect of DCZ accords with the aforementioned behavioral results on fine grasping in the same animals (Figure 2B). As a result, two-way ANOVA on the sensory-evoked SI_{D2} activation revealed significant interaction between the factors of condition (vehicle and DCZ conditions) and hemisphere (DREADD and intact hemispheres) ($p < 0.001$), indicating that the DCZ-induced attenuation of the sensory-evoked SI_{D2} activation was specific to the DREADD-expressing hemisphere and thus was not due to a general effect across hemispheres resulting from off-target action of DCZ. Together, these results demonstrate that sensory-evoked robust BOLD signal in macaques can be reliably and specifically attenuated via inhibitory DREADD.

The DREADD-induced focal SI silencing might also affect the sensory-evoked activity in the downstream network. DCZ administration indeed significantly attenuated hand D2 stimulation-evoked activation of the contralateral posterior parietal cortex (areas 5 and 7) and the secondary somatosensory area (SII) in the DREADD-expressing hemisphere ($p < 0.001$, uncorrected) (Figures 4A and S4A), which were confirmed by ROI analysis ($p < 0.001$, $p < 0.001$, and $p < 0.03$, for areas 5, 7, and SII, respectively, unpaired t test, corrected for multiple comparisons) (Figure 4B). BOLD signal reductions in these remote areas were consistently observed in each of the two monkeys (Figure S4C). These results demonstrate that the effect of focal SI silencing was not local, but extended to the downstream areas in the grasping-related network (Borra et al., 2017; Castiello, 2005; Davare et al., 2011; Jeannerod et al., 1995; Nelissen and Vanduffel, 2011; Rizzolatti and Luppino, 2001; Sharma et al., 2018). In order to examine anatomical and functional connectivity between these affected downstream areas with the SI silencing site, we next conducted the following two different connectivity analyses. First, immunohistochemical analysis showed the expression of co-transduced GFP in the axon terminals of the virus-infected SI_{D2} neurons at the remote-silencing sites in area 5 and SII or their proximity (Figures 4C, top, and S4D), indicating that these regions receive direct anatomical projection from the DREADD-expressing SI_{D2} in the same hemisphere, which was consistent with previous anatomical studies (Burton and Fabri, 1995; Burton et al., 1995). These results suggest that the DCZ-induced activity reduction in these remote areas was, at least in part, due to direct anatomical projection from the DREADD-expressing SI_{D2}. Second, psycho-physiological interaction (PPI) analysis (Friston et al., 1997) with the SI_{D2} activation site of the DREADD hemisphere as a seed region (STAR Methods) revealed that during the contralateral hand D2 stimulation, the DREADD-expressing SI_{D2} was functionally connected with the remote-silencing regions in areas 5, 7, and SII or their proximity in the same hemisphere ($p < 0.05$, FWE-corrected) (Figures 4C, middle, and S4B). These results suggest that the inhibitory effect of DREADD-induced focal SI silencing on the sensory-evoked BOLD signal was not locally restricted to the SI silencing site but extended to the functionally and/or anatomically connected downstream network for grasping behavior (Figure 4C, bottom).

Because the inhibitory DREADD was focally transduced into SI_{D2}, representations of distant body parts, such as the foot, were expected to be unaffected. To assess this prediction, we next examined the BOLD signal in response to sensory stimulation of the foot sole (Figure 5A, left) contralateral to the DREADD hemisphere. Compared with the hand D2 stimulation, cutaneous tactile stimulation of the foot sole significantly activated the contralateral SI at more postero-medial part along the central sulcus ($p < 0.05$, FWE-corrected) (Figure 5A, top middle), which was consistent with the well-known body representation map in the primate SI (Arcaro et al., 2019; Cléry et al., 2020; Kaas, 1983; Krubitzer et al., 2004; Merzenich et al., 1978). In contrast to the DREADD-expressing SI_{D2}, sensory-evoked activity of the SI foot sole region in the same hemisphere was not attenuated following DCZ administration, but rather unexpectedly augmented as compared to the vehicle control condition (Figure 5A, bottom middle). PET analysis revealed that DREADD expression could not be detected within the SI foot sole region even at a lower threshold, where the DREADD at the axon terminal of the SI_{D2} neurons was observed in other cortical and subcortical regions (Figure S5B) (Nagai et al., 2020; Oyama et al., 2021). This result was histologically confirmed as well (data not shown). The DCZ-induced upregulation of the foot sole representation was also observed in the downstream area SII (Figure 5A, right). Subsequent ROI analysis revealed significant increase in the BOLD signal at the foot sole region in both SI and SII following DCZ administration ($p < 0.01$, unpaired t test, corrected for multiple comparisons) (Figure 5B), which was consistently observed in each animal (Figure S5A). These results suggest bidirectional effects of chemogenetic silencing on the operation of the somatosensory network: in addition to the downregulation of the silencing site and its downstream network, focal SI_{D2} silencing also induced upregulation of the network representing distant body parts.

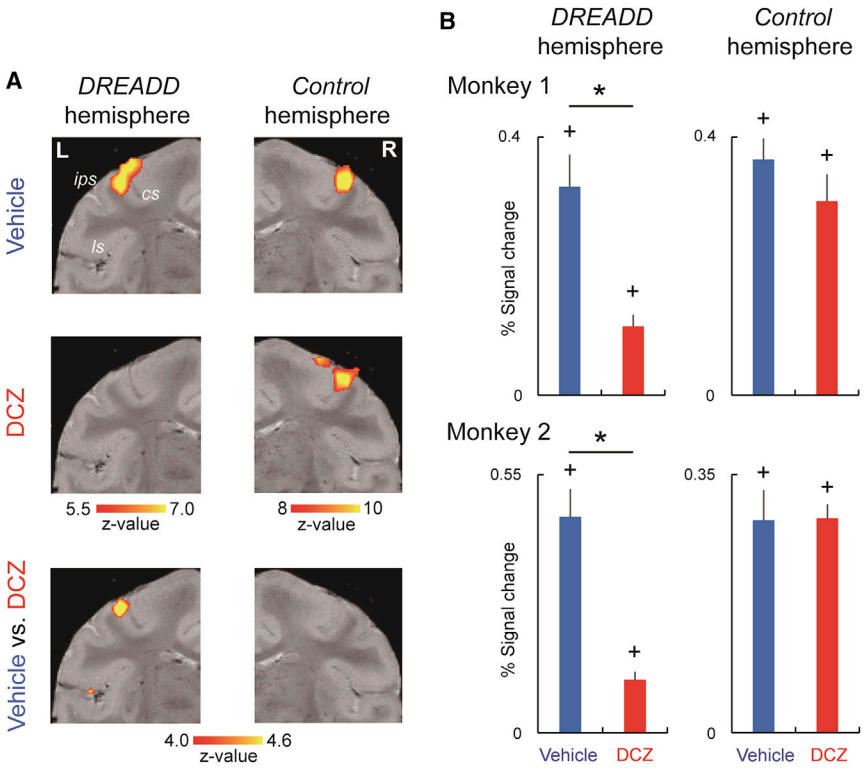

Figure 3. Local attenuation of sensory-evoked BOLD signal in DREADD-expressing SI_{D2}

(A) SI activation in monkey 1 evoked by cutaneous tactile stimulation of the index finger of each hand contralateral (left) and ipsilateral (right) to the DREADD-expressing hemisphere, respectively. SI activations for vehicle (top) and DCZ (middle) conditions, and the difference between them (bottom) were depicted.

(B) Percent signal change calculated for SI ROIs in the contralateral hemisphere to the stimulated hand for each monkey. Results for DREADD-expressing (left) and the opposite (right) hemispheres were depicted. Blue and red columns depict the results in vehicle and DCZ conditions, respectively. Error bars, SEM. *p < 0.001, unpaired t test, corrected for multiple comparisons. +p < 0.001, paired t test for difference from baseline, corrected for multiple comparisons.

See also Figure S3.

The upregulated foot sole representation raised the possibility that the same manipulation might also increase behavioral sensitivity to sensory stimulation of the contralateral foot (Nagasaka et al., 2017, 2020). To test this prediction, we applied a cold (10°C) stimulation, which is known to activate SI in both humans and macaques (Egan et al., 2005; Nagasaka et al., 2017), to the foot sole contralateral to the DREADD-expressing hemisphere, and examined whether focal silencing of the SI hand region behaviorally affects the withdrawal latency of the foot sole from the cold stimulation (Nagasaka et al., 2017, 2020). We found that the withdrawal latency of the contralateral foot sole from the cold stimulation was significantly shortened following DCZ administration ($p < 0.001$, paired t test) (Figure 5C, middle, magenta), suggesting that the inhibitory DREADD-induced upregulation of a distant body part representation indeed was accompanied by a corresponding behavioral hypersensitivity. The specificity of the observed behavioral change was confirmed via the following three different approaches. First, the same DCZ administration in the same experimental session did not induce a significant change in the withdrawal latency when the stimulation temperature was moderate (30°C), for which monkeys were not expected to exhibit withdrawal (Nagasaka et al., 2017, 2020) ($p > 0.6$) (Figure 5C, middle, cyan). As a result, the DCZ-induced change in withdrawal latency was significantly different between the stimulus temperatures (30°C versus 10°C, $p < 0.001$, paired t test). Therefore, the observed behavioral impact was not due to general motor facilitation caused by DCZ itself. Second, we tested whether the ipsilateral foot also shows the DCZ-induced hypersensitivity. In contrast to the contralateral foot, the withdrawal latency of the ipsilateral foot did not significantly change following DCZ administration for either temperature tested (30°C and 10°C) ($p > 0.4$, paired t test), and the changes in the withdrawal latency were not significantly different between the two temperatures ($p > 0.8$) (Figure 5C, right). The results indicate that the hypersensitivity was specific for the contralateral foot. Third, the same DCZ administration did not significantly affect the withdrawal latency for either temperature in a naive monkey (monkey 3, $p > 0.6$), and temperature-dependence of the DCZ-induced latency change was not observed ($p > 0.6$) (Figure S5C). The results again confirmed that the DCZ-induced hypersensitization was not due to DCZ alone, but was exerted via transduced DREADD. Together, concurrent focal SI_{D2} silencing and sensory fMRI revealed DREADD-induced bidirectional changes in the somatosensory network operation underlying the multifaceted behavioral impairments in primates.

DISCUSSION

To elucidate whether and how genetic silencing suppresses and facilitates sensory-evoked network fMRI signal to change relevant behaviors in macaques, we examined the effects of focal SI silencing via inhibitory DREADD on the operation of the somatosensory network and its related behaviors. FMRI-guided DREADD-induced focal silencing of SI_{D2} specifically impaired fine grasping behavior with the contralateral hand D2. The same silencing also attenuated hand D2-mediated sensory-evoked BOLD signal both locally at the DREADD-expressing SI_{D2} and remotely at anatomically and/or functionally connected downstream grasping network. Moreover, the hand region silencing unexpectedly disinhibited foot sole representation in the same hemisphere, which resulted in the corresponding behavioral hypersensitization of the contralateral foot sole.

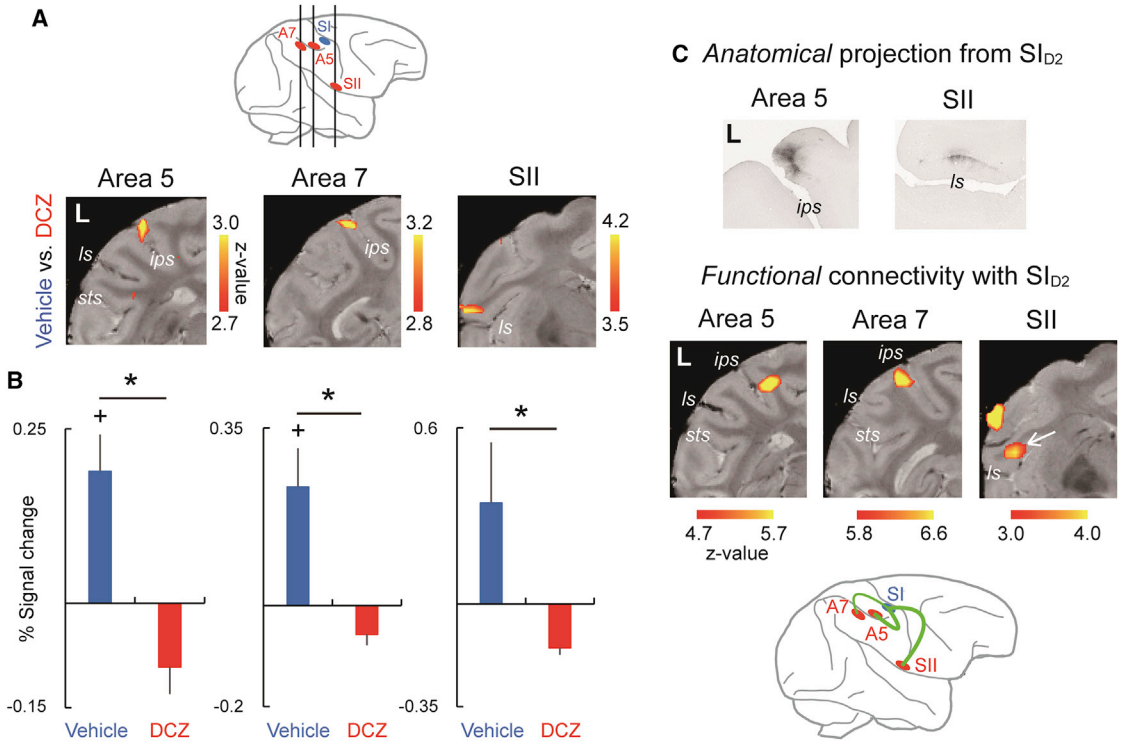

Figure 4. Remote attenuation of sensory-evoked BOLD signal in the downstream grasping network anatomically and/or functionally connected with DREADD-expressing SI_{D2}

(A) DREADD-induced attenuation of the sensory-evoked BOLD signal in the downstream cortical areas of the DREADD-expressed SI in monkey 1. Top, schematic brain with vertical lines depicting approximate AP level of the coronal sections below.

(B) ROI analysis of the sensory-evoked BOLD signal in the regions shown in (A). Data from two monkeys (monkeys 1 and 2) were merged. Error bars, SEM. *$p < 0.03$, unpaired t test, corrected for multiple comparisons. +$p < 0.02$, paired t test for difference from baseline, corrected for multiple comparisons.

(C) Top and middle: anatomical projection from DREADD-expressing SI_{D2} (top) and functional connectivity (PPI) with SI_{D2} (middle) in monkey 1. The projection from SI_{D2} was assessed with immunostaining of the co-transduced GFP at the axon terminals of the virus-infected SI_{D2} neurons. The functional connectivity was assessed using the increased interaction with the ipsilateral SI_{D2} during tactile stimulation of the contralateral hand D2. Bottom: schematic brain showing anatomical/functional connectivity with SI_{D2}.

See also Figure S4.

Together, concurrent chemogenetic silencing and sensory-evoked fMRI unveiled bidirectional network changes underlying the induced behavioral impairments in primates.

To date, a few studies of concurrent genetic neuromodulation and fMRI have been conducted in macaques to investigate changes in BOLD signal or functional connectivity in the resting state (Gerits et al., 2012; Grayson et al., 2016; Ohayon et al., 2013; Vancraeyenest et al., 2020). However, the effect of genetic neuromodulation on task- or sensory-evoked BOLD signal has not been examined despite its importance. Here, we demonstrated that fMRI-guided focal chemogenetics was effective in terms of affecting both the sensory-evoked network BOLD signal and its relevant behaviors in macaques. This is not trivial in primates, as a previous study has reported, only an auxiliary effect of optogenetic stimulation on eliciting BOLD signal in the resting state of macaques (Ohayon et al., 2013), suggesting the difficulty in robustly manipulating BOLD signal reflecting activities of a large population of neurons with genetic tools in macaques (Gerits et al., 2012). This could be a more serious issue in silencing a robustly evoked BOLD signal compared to excitation in the resting state, and indeed no previous study has demonstrated the former in primates. We have overcome this issue by utilizing chemogenetics, with which activities of a given population of neurons can be simultaneously manipulated irrespective of the size of the target region, and thus would be suitable for macaques with much larger brain region involved in a given function compared to other species (Gerits et al., 2012). Although several studies have reported behavioral effects of chemogenetic silencing in macaques (Eldridge et al., 2016; Hayashi et al., 2020; Nagai et al., 2016, 2020; Raper et al., 2019; Upright et al., 2018), only one of these studies performed a physiological assessment of chemogenetic silencing *in vivo*, where the neuronal activity was examined locally at the manipulation target outside the behavioral task context (Hayashi et al., 2020). The present study demonstrated the effect of the same chemogenetic silencing on behavior and its relevant fMRI signal at both local manipulation target and remote regions, thus providing significant advancement in the macaque chemogenetics toward its application to cognitive and/or translational research.

When using a neuromodulation technique, it is critical to verify the specificity of the effect of the modulators: agonists for activating transduced DREADD in the case of chemogenetics

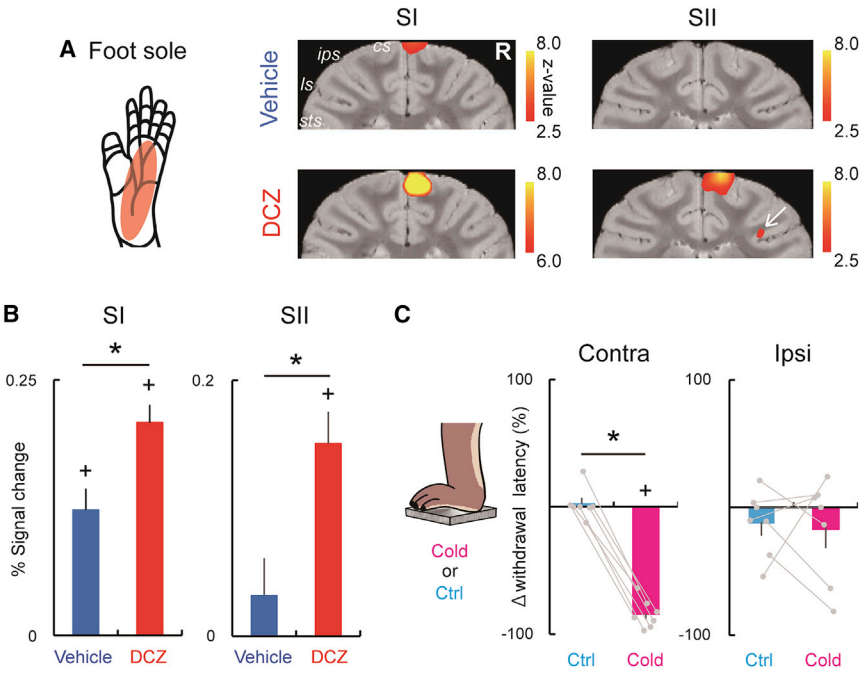

Figure 5. Focal silencing of SI_{D2} upregulated foot representations in the somatosensory network in association with a corresponding behavioral change

(A) Foot sole stimulation-evoked BOLD response in the contralateral SI (middle) and SII (right, white arrow) of the DREADD hemisphere in vehicle (top) and DCZ (bottom) conditions in monkey 2.

(B) Tactile stimulation-induced percent signal change in foot sole region in SI (left) and SII (right) in vehicle (blue) and DCZ (red) conditions. Data from two monkeys (monkeys 1 and 2) were merged. Error bars, SEM. *p < 0.01, unpaired t test, corrected for multiple comparisons. +p < 0.001, paired t test for difference from baseline, corrected for multiple comparisons.

(C) DCZ-induced change in the withdrawal latency of the contralateral (left) and ipsilateral (right) foot sole from cold (magenta) or control (cyan) stimulation in monkey 2. Negative value represents shortened withdrawal latency following DCZ administration. Gray line depicts the performance in each session. Error bars, SEM. *p < 0.001, paired t test. +p < 0.001, for difference between pre and post DCZ administration.

See also Figure S5.

(Eldridge et al., 2016; Gomez et al., 2017; Nagai et al., 2020; Upright and Baxter, 2020). In the present study, we used the recently developed DREADD agonist DCZ, which we demonstrated as being more specific, metabolically stable, and fast-acting agonist *in vivo* compared to the previously used ones (Nagai et al., 2020; see also Bonaventura et al., 2019). The dose of DCZ used for DREADD activation was fixed at 0.1 mg/kg in the present study, as we have shown in a previous study that this dose of DCZ occupied ~80% of the expressed DREADD *in vivo* and was effective in specifically inducing behavioral changes of DREADD-expressing macaques without unwanted changes of behavior or brain activity in naive monkeys (Nagai et al., 2020). Furthermore, our experimental design of unilateral DREADD transduction offered within-animal control condition in the same experimental session for both behavior and fMRI, in which the intact hemisphere and its contralateral hand were involved. DCZ administration with the above dose indeed did not affect the results in the control condition in either behavior (Figure 2B, blue) or fMRI (Figures 3A and 3B, right), ruling out the possibility that the present results were due to side effects of DCZ such as off-target actions via endogenous receptors. Collectively, administration of the highly selective agonist at an adequate dose, unilateral DREADD transduction, and the obtained results in the control conditions thus strongly suggest that the present results indeed reflected specific neuromodulation via transduced DREADD.

In the present study, DREADD-induced silencing of unilateral SI_{D2} impaired fine grasping with the contralateral hand D2, which is consistent with previous behavioral studies with more conventional approaches including permanent lesion or transient pharmacological inactivation of the macaque SI (Asanuma and Arissian, 1984; Brochier et al., 1999; Hikosaka et al., 1985). However, the impact of behaviorally efficacious focal SI inactivation on the relevant sensory-evoked network signal has not been examined. The cortical somatosensory system involved in object grasping is not restricted to SI, but also a broader network including SII and posterior parietal regions such as areas 5 and 7 (Borra et al., 2017; Castiello, 2005; Davare et al., 2011; Jeannerod et al., 1995; Nelissen and Vanduffel, 2011; Padberg et al., 2010; Rizzolatti and Luppino, 2001; Sharma et al., 2018). Indeed, inactivation of these areas leads to impaired grasping and/or other tactile deficiencies (Brochier et al., 1999; Carlson and Burton, 1988; Gallese et al., 1994; Murray and Mishkin, 1984; Padberg et al., 2010). The present results that focal SI silencing led to the extended downregulation of the above-mentioned grasping network would thus suggest the neural underpinnings of the observed behavioral impairment of fine grasping caused by the same silencing in the same animals. It has long been postulated that manual dexterity impairment following SI inactivation is simply due to local dysfunction of SI itself or SI-MI interaction (Brochier et al., 1999; Hikosaka et al., 1985). The present results thus suggest a novel possibility that the impact of SI inactivation on fine grasping behavior might be, at least in part, due to more extended downregulation of the anatomically and/or functionally connected grasping network. Combining behavioral testing with fMRI under the same neuromodulation is thus critical to the manifestation of changes in the network operation underlying the induced behavioral impairment. However, because the present study was designed to combine fMRI for passive hand stimulation under light sedation and behavioral assessment of active grasping in awake condition, the fMRI results would have provided only a portion of the functional network used in the behavior (Sharma et al., 2018). Awake fMRI during object grasping task (Nelissen and Vanduffel, 2011; Sharma et al., 2018) concurrent with neuromodulation would thus be required for more direct comparison

between the effects of focal SI silencing on behavior and network operation in future studies. Furthermore, because we defined SI_{D2} without subtraction of the activation in response to other digits, the silenced region might have included their representations as well. Spatially more precise neuromodulation confined to a single digit representation (Xu et al., 2019) and investigations of its effect on both behavior and network function would also be important issues in future studies.

We also demonstrated that focal silencing of the SI hand region resulted in unexpected upregulation of foot sole representation in the same hemisphere and corresponding behavioral hypersensitivity to cold stimulus on the contralateral foot sole (Figure 5). A previous human fMRI study showed that sensory-evoked activation of a given body-part representation in SI was associated with suppression of regions representing distant body parts in SI of the same hemisphere (Tal et al., 2017). This suggests that representations of different body parts in SI are not independent of each other, but exert mutually inhibitory interaction, leading to an increased signal-to-noise ratio of the sensory representation in response to tactile stimulation of a given body part (Tal et al., 2017). Inhibitory interdependence between the SI representations of different body parts has also been observed at the level of single neurons in macaques (Lipton et al., 2010). However, causal evidence on such interaction and its behavioral impact has remained lacking. Therefore, the present results would provide, although partial, the first causal evidence on the inhibitory interaction between different body part representations in terms of both physiology and behavior in primates. Similar mutual inhibition within area has also been reported in the primary visual cortex in macaques (Chernov et al., 2018; Shmuel et al., 2006) and thus might be a general mechanism especially in primary sensory cortices across modalities (Tal et al., 2017). The observed effects could not be attributable to spatially less confined DREADD expression extended to the foot sole region (Figure S5B). Although the result would not rule out the possibility of a weak expression of DREADD at the axon terminal of SI_{D2} neurons projecting to the foot sole region, the effect would more likely be due to indirect interaction via other cortical or subcortical regions (Blankenburg et al., 2008). From another point of view, previous studies on concurrent inhibitory neuromodulation and fMRI have revealed not only suppression but also facilitation of remote network communications in the resting state (Chen et al., 2013; Grayson et al., 2016; Vancraeyenest et al., 2020). However, behavioral effects corresponding to both of the bidirectional neural changes caused by a single manipulation have not been examined. Although further studies would be required to elucidate the whole picture including the DCZ-induced change in the sensitivity of hands and specific circuit mechanisms underlying the mutual inhibition between representations of different body parts (Tal et al., 2017), the present results demonstrate that focal chemogenetic silencing in macaques can induce behaviorally relevant bidirectional changes of neuronal activity in remote regions, which could be identified via concurrent silencing and sensory-evoked fMRI.

In summary, we demonstrated here that fMRI-guided focal chemogenetic silencing bidirectionally changes sensory-evoked network signal with accompanying impairment of corresponding behaviors in macaques. In contrast to conventional perturbation, chemogenetic silencing offers minimally invasive repetitive manipulations of virtually the same and genetically characterized neuronal population without physical damage to the manipulation target tissue or non-negligible fMRI signal loss/distortion due to additional device/implantation. These advantages would also allow for repetitive and reproducible silencing in an fMRI and its follow-up electrophysiological investigation at a remote silencing site to elucidate its neuronal underpinning in the same animal. Such an approach would lead to a multi-scale understanding of the causal network operation underlying various higher brain functions in non-human primates, translationally providing deeper insights into the corresponding human brain functions in health and disease.

STAR★METHODS

Detailed methods are provided in the online version of this paper and include the following:

- KEY RESOURCES TABLE
- RESOURCE AVAILABILITY
  - Lead contact
  - Materials availability
  - Data and code availability
- EXPERIMENTAL MODEL AND SUBJECT DETAILS
- METHOD DETAILS
  - Viral vector production
  - AAV vector injection into fMRI-defined SI_{D2}
  - Histology and immunostaining
  - *In vivo* PET visualization of DREADD expression
  - Behavioral tests
  - MRI scanning
  - MRI data analyses

SUPPLEMENTAL INFORMATION

Supplemental information can be found online at https://doi.org/10.1016/j.neuron.2021.08.032.

ACKNOWLEDGMENTS

We thank J. Kamei, Y. Sugii, R. Yamaguchi, Y. Matsuda, T. Kokufuta, A. Maruyama, Y. Ozawa, S. Shibata, N. Nitta, M. Nakano, and M. Fujiwara for technical assistance, and Dr. N. Goda for helpful discussions. We also thank Dr. S. Hiura for production of the 3D model brains. This research is supported by MEXT/JSPS KAKENHI (JP15H05917 and JP20H05955 to T.M. and JP17H02219 to T.H.), by AMED (17dm0107066h to I.A., JP18dm0207003 to M.T., JP18dm0307021 to K.I., JP21dm0307007 to T.H., and JP20dm0107146 to T.M.), by the cooperative research program at PRI, Kyoto University, and by National Bio-Resource Project "Japanese Monkeys" of MEXT, Japan.

AUTHOR CONTRIBUTIONS

T.H. designed the study and wrote the first draft of the manuscript. T.H., Y.N., and Y.H. conducted experiments. T.H. and Y.N. analyzed the data. All authors finalized the manuscript.

DECLARATION OF INTERESTS

The authors declare no competing interests.

INCLUSION AND DIVERSITY

We worked to ensure sex balance in the selection of non-human subjects. While citing references scientifically relevant for this work, we also actively worked to promote gender balance in our reference list.

Received: March 8, 2021
Revised: July 1, 2021
Accepted: August 26, 2021
Published: October 20, 2021

SUPPORTING CITATIONS

The following references appear in the supplemental information: Fogassi et al. (2001); Gerbella et al. (2017); Lega et al. (2020).

REFERENCES

Arcaro, M.J., Schade, P.F., and Livingstone, M.S. (2019). Body map proto-organization in newborn macaques. Proc. Natl. Acad. Sci. USA *116*, 24861–24871.

Asanuma, H., and Arissian, K. (1984). Experiments on functional role of peripheral input to motor cortex during voluntary movements in the monkey. J. Neurophysiol. *52*, 212–227.

Bergmann, T.O., and Hartwigsen, G. (2021). Inferring Causality from Noninvasive Brain Stimulation in Cognitive Neuroscience. J. Cogn. Neurosci. *33*, 195–225.

Bestmann, S., Swayne, O., Blankenburg, F., Ruff, C.C., Haggard, P., Weiskopf, N., Josephs, O., Driver, J., Rothwell, J.C., and Ward, N.S. (2008). Dorsal premotor cortex exerts state-dependent causal influences on activity in contralateral primary motor and dorsal premotor cortex. Cereb. Cortex *18*, 1281–1291.

Blankenburg, F., Ruff, C.C., Bestmann, S., Bjoertomt, O., Eshel, N., Josephs, O., Weiskopf, N., and Driver, J. (2008). Interhemispheric effect of parietal TMS on somatosensory response confirmed directly with concurrent TMS-fMRI. J. Neurosci. *28*, 13202–13208.

Bogadhi, A.R., Bollimunta, A., Leopold, D.A., and Krauzlis, R.J. (2019). Spatial Attention Deficits Are Causally Linked to an Area in Macaque Temporal Cortex. Curr. Biol. *29*, 726–736.e4.

Bonaventura, J., Eldridge, M.A.G., Hu, F., Gomez, J.L., Sanchez-Soto, M., Abramyan, A.M., Lam, S., Boehm, M.A., Ruiz, C., Farrell, M.R., et al. (2019). High-potency ligands for DREADD imaging and activation in rodents and monkeys. Nat. Commun. *10*, 4627.

Borra, E., Gerbella, M., Rozzi, S., and Luppino, G. (2017). The macaque lateral grasping network: A neural substrate for generating purposeful hand actions. Neurosci. Biobehav. Rev. *75*, 65–90.

Brinkman, C. (1984). Supplementary motor area of the monkey's cerebral cortex: short- and long-term deficits after unilateral ablation and the effects of subsequent callosal section. J. Neurosci. *4*, 918–929.

Brinkman, J., and Kuypers, H.G. (1973). Cerebral control of contralateral and ipsilateral arm, hand and finger movements in the split-brain rhesus monkey. Brain *96*, 653–674.

Brochier, T., Boudreau, M.J., Paré, M., and Smith, A.M. (1999). The effects of muscimol inactivation of small regions of motor and somatosensory cortex on independent finger movements and force control in the precision grip. Exp. Brain Res. *128*, 31–40.

Burton, H., and Fabri, M. (1995). Ipsilateral intracortical connections of physiologically defined cutaneous representations in areas 3b and 1 of macaque monkeys: projections in the vicinity of the central sulcus. J. Comp. Neurol. *355*, 508–538.

Burton, H., Fabri, M., and Alloway, K. (1995). Cortical areas within the lateral sulcus connected to cutaneous representations in areas 3b and 1: a revised interpretation of the second somatosensory area in macaque monkeys. J. Comp. Neurol. *355*, 539–562.

Carlson, M., and Burton, H. (1988). Recovery of tactile function after damage to primary or secondary somatic sensory cortex in infant Macaca mulatta. J. Neurosci. *8*, 833–859.

Carrera, E., and Tononi, G. (2014). Diaschisis: past, present, future. Brain *137*, 2408–2422.

Castiello, U. (2005). The neuroscience of grasping. Nat. Rev. Neurosci. *6*, 726–736.

Chen, L.M., Turner, G.H., Friedman, R.M., Zhang, N., Gore, J.C., Roe, A.W., and Avison, M.J. (2007). High-resolution maps of real and illusory tactile activation in primary somatosensory cortex in individual monkeys with functional magnetic resonance imaging and optical imaging. J. Neurosci. *27*, 9181–9191.

Chen, A.C., Oathes, D.J., Chang, C., Bradley, T., Zhou, Z.W., Williams, L.M., Glover, G.H., Deisseroth, K., and Etkin, A. (2013). Causal interactions between fronto-parietal central executive and default-mode networks in humans. Proc. Natl. Acad. Sci. USA *110*, 19944–19949.

Chernov, M.M., Friedman, R.M., Chen, G., Stoner, G.R., and Roe, A.W. (2018). Functionally specific optogenetic modulation in primate visual cortex. Proc. Natl. Acad. Sci. USA *115*, 10505–10510.

Cléry, J.C., Hori, Y., Schaeffer, D.J., Gati, J.S., Pruszynski, J.A., and Everling, S. (2020). Whole brain mapping of somatosensory responses in awake marmosets investigated with ultra-high-field fMRI. J. Neurophysiol. *124*, 1900–1913.

Davare, M., Rothwell, J.C., and Lemon, R.N. (2010). Causal connectivity between the human anterior intraparietal area and premotor cortex during grasp. Curr. Biol. *20*, 176–181.

Davare, M., Kraskov, A., Rothwell, J.C., and Lemon, R.N. (2011). Interactions between areas of the cortical grasping network. Curr. Opin. Neurobiol. *21*, 565–570.

Deffains, M., Nguyen, T.H., Orignac, H., Biendon, N., Dovero, S., Bezard, E., and Boraud, T. (2021). In vivo electrophysiological validation of DREADD-based modulation of pallidal neurons in the non-human primate. Eur. J. Neurosci. *53*, 2192–2204.

Dutta, A., Kambi, N., Raghunathan, P., Khushu, S., and Jain, N. (2014). Large-scale reorganization of the somatosensory cortex of adult macaque monkeys revealed by fMRI. Brain Struct. Funct. *219*, 1305–1320.

Egan, G.F., Johnson, J., Farrell, M., McAllen, R., Zamarripa, F., McKinley, M.J., Lancaster, J., Denton, D., and Fox, P.T. (2005). Cortical, thalamic, and hypothalamic responses to cooling and warming the skin in awake humans: a positron-emission tomography study. Proc. Natl. Acad. Sci. USA *102*, 5262–5267.

Ekstrom, L.B., Roelfsema, P.R., Arsenault, J.T., Bonmassar, G., and Vanduffel, W. (2008). Bottom-up dependent gating of frontal signals in early visual cortex. Science *321*, 414–417.

El-Shamayleh, Y., and Horwitz, G.D. (2019). Primate optogenetics: Progress and prognosis. Proc. Natl. Acad. Sci. USA *116*, 26195–26203.

Eldridge, M.A., Lerchner, W., Saunders, R.C., Kaneko, H., Krausz, K.W., Gonzalez, F.J., Ji, B., Higuchi, M., Minamimoto, T., and Richmond, B.J. (2016). Chemogenetic disconnection of monkey orbitofrontal and rhinal cortex reversibly disrupts reward value. Nat. Neurosci. *19*, 37–39.

Fogassi, L., Gallese, V., Buccino, G., Craighero, L., Fadiga, L., and Rizzolatti, G. (2001). Cortical mechanism for the visual guidance of hand grasping movements in the monkey: A reversible inactivation study. Brain *124*, 571–586.

Frahm, J., Haase, A., and Matthaei, D. (1986). Rapid three-dimensional MR imaging using the FLASH technique. J. Comput. Assist. Tomogr. *10*, 363–368.

Friston, K.J., Buechel, C., Fink, G.R., Morris, J., Rolls, E., and Dolan, R.J. (1997). Psychophysiological and modulatory interactions in neuroimaging. Neuroimage *6*, 218–229.

Gallese, V., Murata, A., Kaseda, M., Niki, N., and Sakata, H. (1994). Deficit of hand preshaping after muscimol injection in monkey parietal cortex. Neuroreport *5*, 1525–1529.

Galvan, A., Caiola, M.J., and Albaugh, D.L. (2018). Advances in optogenetic and chemogenetic methods to study brain circuits in non-human primates. J. Neural Transm. (Vienna) *125*, 547–563.

Gerbella, M., Rozzi, S., and Rizzolatti, G. (2017). The extended object-grasping network. Exp. Brain Res. *235*, 2903–2916.

Gerits, A., Farivar, R., Rosen, B.R., Wald, L.L., Boyden, E.S., and Vanduffel, W. (2012). Optogenetically induced behavioral and functional network changes in primates. Curr. Biol. *22*, 1722–1726.

Gomez, J.L., Bonaventura, J., Lesniak, W., Mathews, W.B., Sysa-Shah, P., Rodriguez, L.A., Ellis, R.J., Richie, C.T., Harvey, B.K., Dannals, R.F., et al. (2017). Chemogenetics revealed: DREADD occupancy and activation via converted clozapine. Science *357*, 503–507.

Grayson, D.S., Bliss-Moreau, E., Machado, C.J., Bennett, J., Shen, K., Grant, K.A., Fair, D.A., and Amaral, D.G. (2016). The Rhesus Monkey Connectome Predicts Disrupted Functional Networks Resulting from Pharmacogenetic Inactivation of the Amygdala. Neuron *91*, 453–466.

Hayashi, T., Konishi, S., Hasegawa, I., and Miyashita, Y. (1999). Short communication: mapping of somatosensory cortices with functional magnetic resonance imaging in anaesthetized macaque monkeys. Eur. J. Neurosci. *11*, 4451–4456.

Hayashi, T., Akikawa, R., Kawasaki, K., Egawa, J., Minamimoto, T., Kobayashi, K., Kato, S., Hori, Y., Nagai, Y., Iijima, A., et al. (2020). Macaques Exhibit Implicit Gaze Bias Anticipating Others' False-Belief-Driven Actions via Medial Prefrontal Cortex. Cell Rep. *30*, 4433–4444.e5.

Hikosaka, O., Tanaka, M., Sakamoto, M., and Iwamura, Y. (1985). Deficits in manipulative behaviors induced by local injections of muscimol in the first somatosensory cortex of the conscious monkey. Brain Res. *325*, 375–380.

Jeannerod, M., Michel, F., and Prablanc, C. (1984). The control of hand movements in a case of hemianaesthesia following a parietal lesion. Brain *107*, 899–920.

Jeannerod, M., Arbib, M.A., Rizzolatti, G., and Sakata, H. (1995). Grasping objects: the cortical mechanisms of visuomotor transformation. Trends Neurosci. *18*, 314–320.

Kaas, J.H. (1983). What, if anything, is SI? Organization of first somatosensory area of cortex. Physiol. Rev. *63*, 206–231.

Kimura, K., Nagai, Y., Hatanaka, G., Fang, Y., Zheng, A., Fujiwara, M., Nakano, M., Hori, Y., Takeuchi, R., Inagaki, M., et al. (2021). A mosaic adeno-associated virus vector as a versatile tool that exhibits high levels of transgene expression and neuron specificity in primate brain. bioRxiv. https://doi.org/10.1101/2021.07.18.452859.

Klink, P.C., Aubry, J.F., Ferrera, V.P., Fox, A.S., Froudist-Walsh, S., Jarraya, B., Konofagou, E.E., Krauzlis, R.J., Messinger, A., Mitchell, A.S., et al. (2021). Combining brain perturbation and neuroimaging in non-human primates. Neuroimage *235*, 118017.

Krubitzer, L., Huffman, K.J., Disbrow, E., and Recanzone, G. (2004). Organization of area 3a in macaque monkeys: contributions to the cortical phenotype. J. Comp. Neurol. *471*, 97–111.

Lega, C., Pirruccio, M., Bicego, M., Parmigiani, L., Chelazzi, L., and Cattaneo, L. (2020). The Topography of Visually Guided Grasping in the Premotor Cortex: A Dense-Transcranial Magnetic Stimulation (TMS) Mapping Study. J. Neurosci. *40*, 6790–6800.

Lerchner, W., Corgiat, B., Der Minassian, V., Saunders, R.C., and Richmond, B.J. (2014). Injection parameters and virus dependent choice of promoters to improve neuron targeting in the nonhuman primate brain. Gene Ther. *21*, 233–241.

Lipton, M.L., Fu, K.M., Branch, C.A., and Schroeder, C.E. (2006). Ipsilateral hand input to area 3b revealed by converging hemodynamic and electrophysiological analyses in macaque monkeys. J. Neurosci. *26*, 180–185.

Lipton, M.L., Liszewski, M.C., O'Connell, M.N., Mills, A., Smiley, J.F., Branch, C.A., Isler, J.R., and Schroeder, C.E. (2010). Interactions within the hand representation in primary somatosensory cortex of primates. J. Neurosci. *30*, 15895–15903.

McLaren, D.G., Kosmatka, K.J., Oakes, T.R., Kroenke, C.D., Kohama, S.G., Matochik, J.A., Ingram, D.K., and Johnson, S.C. (2009). A population-average MRI-based atlas collection of the rhesus macaque. Neuroimage *45*, 52–59.

Merzenich, M.M., Kaas, J.H., Sur, M., and Lin, C.S. (1978). Double representation of the body surface within cytoarchitectonic areas 3b and 1 in "SI" in the owl monkey (Aotus trivirgatus). J. Comp. Neurol. *181*, 41–73.

Miyamoto, K., Osada, T., Setsuie, R., Takeda, M., Tamura, K., Adachi, Y., and Miyashita, Y. (2017). Causal neural network of metamemory for retrospection in primates. Science *355*, 188–193.

Moeller, S., Freiwald, W.A., and Tsao, D.Y. (2008). Patches with links: a unified system for processing faces in the macaque temporal lobe. Science *320*, 1355–1359.

Murray, E.A., and Mishkin, M. (1984). Relative contributions of SII and area 5 to tactile discrimination in monkeys. Behav. Brain Res. *11*, 67–83.

Nagai, Y., Kikuchi, E., Lerchner, W., Inoue, K.I., Ji, B., Eldridge, M.A., Kaneko, H., Kimura, Y., Oh-Nishi, A., Hori, Y., et al. (2016). PET imaging-guided chemogenetic silencing reveals a critical role of primate rostromedial caudate in reward evaluation. Nat. Commun. *7*, 13605.

Nagai, Y., Miyakawa, N., Takuwa, H., Hori, Y., Oyama, K., Ji, B., Takahashi, M., Huang, X.P., Slocum, S.T., DiBerto, J.F., et al. (2020). Deschloroclozapine, a potent and selective chemogenetic actuator enables rapid neuronal and behavioral modulations in mice and monkeys. Nat. Neurosci. *23*, 1157–1167.

Nagasaka, K., Yamanaka, K., Ogawa, S., Takamatsu, H., and Higo, N. (2017). Brain activity changes in a macaque model of oxaliplatin-induced neuropathic cold hypersensitivity. Sci. Rep. *7*, 4305.

Nagasaka, K., Takashima, I., Matsuda, K., and Higo, N. (2020). Brain activity changes in a monkey model of central post-stroke pain. Exp. Neurol. *323*, 113096.

Nelissen, K., and Vanduffel, W. (2011). Grasping-related functional magnetic resonance imaging brain responses in the macaque monkey. J. Neurosci. *31*, 8220–8229.

Nelissen, K., Borra, E., Gerbella, M., Rozzi, S., Luppino, G., Vanduffel, W., Rizzolatti, G., and Orban, G.A. (2011). Action observation circuits in the macaque monkey cortex. J. Neurosci. *31*, 3743–3756.

Nishimura, Y., Onoe, H., Morichika, Y., Perfiliev, S., Tsukada, H., and Isa, T. (2007). Time-dependent central compensatory mechanisms of finger dexterity after spinal cord injury. Science *318*, 1150–1155.

Ohayon, S., Grimaldi, P., Schweers, N., and Tsao, D.Y. (2013). Saccade modulation by optical and electrical stimulation in the macaque frontal eye field. J. Neurosci. *33*, 16684–16697.

Oyama, K., Hori, Y., Nagai, Y., Miyakawa, N., Mimura, K., Hirabayashi, T., Inoue, K.I., Suhara, T., Takada, M., Higuchi, M., and Minamimoto, T. (2021). Chemogenetic dissection of the primate prefronto-subcortical pathways for working memory and decision-making. Sci. Adv. *7*. https://doi.org/10.1126/sciadv.abg4246.

Padberg, J., Recanzone, G., Engle, J., Cooke, D., Goldring, A., and Krubitzer, L. (2010). Lesions in posterior parietal area 5 in monkeys result in rapid behavioral and cortical plasticity. J. Neurosci. *30*, 12918–12935.

Raper, J., Murphy, L., Richardson, R., Romm, Z., Kovacs-Balint, Z., Payne, C., and Galvan, A. (2019). Chemogenetic Inhibition of the Amygdala Modulates Emotional Behavior Expression in Infant Rhesus Monkeys. eNeuro *6*, ENEURO.0360-19.2019.

Rizzolatti, G., and Luppino, G. (2001). The cortical motor system. Neuron *31*, 889–901.

Rocchi, F., Oya, H., Balezeau, F., Billig, A.J., Kocsis, Z., Jenison, R.L., Nourski, K.V., Kovach, C.K., Steinschneider, M., Kikuchi, Y., et al. (2021). Common fronto-temporal effective connectivity in humans and monkeys. Neuron *109*, 852–868.e8.

Roth, B.L. (2016). DREADDs for Neuroscientists. Neuron *89*, 683–694.

Rouiller, E.M., Yu, X.H., Moret, V., Tempini, A., Wiesendanger, M., and Liang, F. (1998). Dexterity in adult monkeys following early lesion of the motor cortical hand area: the role of cortex adjacent to the lesion. Eur. J. Neurosci. *10*, 729–740.

Sani, I., Stemmann, H., Caron, B., Bullock, D., Stemmler, T., Fahle, M., Pestilli, F., and Freiwald, W.A. (2021). The human endogenous attentional control network includes a ventro-temporal cortical node. Nat. Commun. *12*, 360.

Sawada, M., Kato, K., Kunieda, T., Mikuni, N., Miyamoto, S., Onoe, H., Isa, T., and Nishimura, Y. (2015). Function of the nucleus accumbens in motor control during recovery after spinal cord injury. Science *350*, 98–101.

Schmid, M.C., Mrowka, S.W., Turchi, J., Saunders, R.C., Wilke, M., Peters, A.J., Ye, F.Q., and Leopold, D.A. (2010). Blindsight depends on the lateral geniculate nucleus. Nature *466*, 373–377.

Sharma, S., Fiave, P.A., and Nelissen, K. (2018). Functional MRI Responses to Passive, Active, and Observed Touch in Somatosensory and Insular Cortices of the Macaque Monkey. J. Neurosci. *38*, 3689–3707.

Shmuel, A., Augath, M., Oeltermann, A., and Logothetis, N.K. (2006). Negative functional MRI response correlates with decreases in neuronal activity in monkey visual area V1. Nat. Neurosci. *9*, 569–577.

Silvanto, J., Muggleton, N., and Walsh, V. (2008). State-dependency in brain stimulation studies of perception and cognition. Trends Cogn. Sci. *12*, 447–454.

Tal, Z., Geva, R., and Amedi, A. (2017). Positive and Negative Somatotopic BOLD Responses in Contralateral Versus Ipsilateral Penfield Homunculus. Cereb. Cortex *27*, 962–980.

Thompson, A., Murphy, D., Dell'Acqua, F., Ecker, C., McAlonan, G., Howells, H., Baron-Cohen, S., Lai, M.C., Lombardo, M.V., and Catani, M.; MRC AIMS Consortium, and Marco Catani (2017). Impaired Communication Between the Motor and Somatosensory Homunculus Is Associated With Poor Manual Dexterity in Autism Spectrum Disorder. Biol. Psychiatry *81*, 211–219.

Tolias, A.S., Sultan, F., Augath, M., Oeltermann, A., Tehovnik, E.J., Schiller, P.H., and Logothetis, N.K. (2005). Mapping cortical activity elicited with electrical microstimulation using FMRI in the macaque. Neuron *48*, 901–911.

Tremblay, S., Acker, L., Afraz, A., Albaugh, D.L., Amita, H., Andrei, A.R., Angelucci, A., Aschner, A., Balan, P.F., Basso, M.A., et al. (2020). An Open Resource for Non-human Primate Optogenetics. Neuron *108*, 1075–1090.e6.

Upright, N.A., and Baxter, M.G. (2020). Effect of chemogenetic actuator drugs on prefrontal cortex-dependent working memory in nonhuman primates. Neuropsychopharmacology *45*, 1793–1798.

Upright, N.A., Brookshire, S.W., Schnebelen, W., Damatac, C.G., Hof, P.R., Browning, P.G.F., Croxson, P.L., Rudebeck, P.H., and Baxter, M.G. (2018). Behavioral Effect of Chemogenetic Inhibition Is Directly Related to Receptor Transduction Levels in Rhesus Monkeys. J. Neurosci. *38*, 7969–7975.

Van Dromme, I.C., Premereur, E., Verhoef, B.E., Vanduffel, W., and Janssen, P. (2016). Posterior Parietal Cortex Drives Inferotemporal Activations During Three-Dimensional Object Vision. PLoS Biol. *14*, e1002445.

Vancraeyenest, P., Arsenault, J.T., Li, X., Zhu, Q., Kobayashi, K., Isa, K., Isa, T., and Vanduffel, W. (2020). Selective Mesoaccumbal Pathway Inactivation Affects Motivation but Not Reinforcement-Based Learning in Macaques. Neuron *108*, 568–581.e6.

Vanduffel, W., Zhu, Q., and Orban, G.A. (2014). Monkey cortex through fMRI glasses. Neuron *83*, 533–550.

Verhagen, L., Gallea, C., Folloni, D., Constans, C., Jensen, D.E., Ahnine, H., Roumazeilles, L., Santin, M., Ahmed, B., Lehericy, S., et al. (2019). Offline impact of transcranial focused ultrasound on cortical activation in primates. eLife *8*, e40541.

Wang, Z., Chen, L.M., Négyessy, L., Friedman, R.M., Mishra, A., Gore, J.C., and Roe, A.W. (2013). The relationship of anatomical and functional connectivity to resting-state connectivity in primate somatosensory cortex. Neuron *78*, 1116–1126.

Wilke, M., Kagan, I., and Andersen, R.A. (2012). Functional imaging reveals rapid reorganization of cortical activity after parietal inactivation in monkeys. Proc. Natl. Acad. Sci. USA *109*, 8274–8279.

Xu, A.G., Qian, M., Tian, F., Xu, B., Friedman, R.M., Wang, J., Song, X., Sun, Y., Chernov, M.M., Cayce, J.M., et al. (2019). Focal infrared neural stimulation with high-field functional MRI: A rapid way to map mesoscale brain connectomes. Sci. Adv. *5*, eaau7046.

Yan, X., Telu, S., Dick, R.M., Liow, J.S., Zanotti-Fregonara, P., Morse, C.L., Manly, L.S., Gladding, R.L., Shrestha, S., Lerchner, W., et al. (2021). [(11)C]deschloroclozapine is an improved PET radioligand for quantifying a human muscarinic DREADD expressed in monkey brain. J. Cereb. Blood Flow Metab. Published online April 14, 2021. https://doi.org/10.1177/0271678X211007949.

Yang, P.F., Phipps, M.A., Newton, A.T., Chaplin, V., Gore, J.C., Caskey, C.F., and Chen, L.M. (2018). Neuromodulation of sensory networks in monkey brain by focused ultrasound with MRI guidance and detection. Sci. Rep. *8*, 7993.

Yang, P.F., Phipps, M.A., Jonathan, S., Newton, A.T., Byun, N., Gore, J.C., Grissom, W.A., Caskey, C.F., and Chen, L.M. (2021). Bidirectional and state-dependent modulation of brain activity by transcranial focused ultrasound in non-human primates. Brain Stimul. *14*, 261–272.

STAR★METHODS

KEY RESOURCES TABLE

REAGENT or RESOURCE	SOURCE	IDENTIFIER
Antibodies		
GFP Recombinant Rabbit Monoclonal Antibody	Thermo Fisher Scientific	Cat# G10362; RRID:AB_2536526
Biotin-SP (long spacer) AffiniPure Donkey Anti-Rabbit IgG (H+L)	Jackson ImmunoResearch Labs	Cat# 711-065-152; RRID:AB_2340593
Bacterial and virus strains		
AAV2.1-hSyn-hM4Di-IRES2-AcGFP	This paper	N/A
AAV2-CMV-hM4Di	This paper	N/A
AAV2-CMV-AcGFP	This paper	N/A
Chemicals, peptides, and recombinant proteins		
Deschloroclozapine (DCZ)	MedChemExpress	Cat# HY-42110
Critical commercial assays		
Avidin-biotin-peroxidase complex	ABC Elite	Vector Laboratories
Experimental models: Organisms/strains		
Macaca fuscata	National BioResource Project	N/A
Software and algorithms		
MATLAB	MathWorks	*RRID*:SCR_001622
PMOD Software	PMOD Technologies	*RRID*:SCR_016547
SPM	Welcome Trust Centre for Neuroimaging	12.0
MarsBaR	N/A	RRID:SCR_009605
Other		
CT scanner	J. MORITA CO.	Accuitomo170
10-μl syringe	MPI	NanoFil Syringe
Motorized microinjector	KD Scientific	Legato130
Motorized microinjector	WPI	UMP3T-2
Manipulator	David Kopf	model 1460
Operating microscope	Leica Microsystems	Leica M220
Charge-coupled device (CCD) camera	Keyence	Biorevo
PET scanner	Siemens Medical Solutions	microPET Focus 220
Cool Plate	AS ONE	SCP-85
7T MRI scanner (Magnet)	KOBELCO/JASTEC	N/A
7T MRI scanner (Spectrometer and console)	Bruker Biospin	AVANCE-I
Volume resonator	Takashima	N/A
4-ch phased array receiver coil	Rapid Biomedical	N/A
Taq-Man technology	Life Technologies	N/A

RESOURCE AVAILABILITY

Lead contact

Further information and requests for resources and reagents should be directed to and will be fulfilled by the lead contact, Toshiyuki Hirabayashi (hirabayashi.toshiyuki@qst.go.jp).

Materials availability

This study did not generate new unique reagents.

Data and code availability

All data reported in this paper will be shared by the lead contact upon request.

This paper does not report original code.

Any additional information required to reanalyze the data reported in this paper is available from the lead contact upon request.

EXPERIMENTAL MODEL AND SUBJECT DETAILS

In total, three Japanese macaque monkeys (*Macaca fuscata,* one male and two females, weight: 5 to 8 kg, Age: 5 to 10 years) were used for experiments. Inhibitory DREADD (hM4Di) was expressed in the unilateral SI_{D2} in two monkeys (left for monkey 1, right for monkey 2) via injections of AAV vectors encoding hM4Di. These two monkeys participated in SI_{D2} localizer fMRI, DCZ-PET for *in vivo* visualization of the expressed DREADD (Nagai et al., 2020), and chemogenetic SI_{D2} silencing concurrent with fMRI and behavioral tests. One monkey without DREADD gene induction (monkey 3) participated in behavioral tests of cold stimulus sensitivity applied to the foot sole as a naive control monkey. All experimental protocols were in full compliance with the Guide for the Care and Use of Laboratory Animals (National Research Council of the US National Academy of Sciences) and were approved by the Animal Ethics Committee of the National Institutes of Quantum and Radiological Science and Technology.

METHOD DETAILS

Viral vector production

Viral vectors (AAV2.1-hSyn-hM4Di-IRES2-AcGFP (Kimura et al., 2021), AAV2-CMV-hM4Di, and AAV2-CMV-AcGFP) were produced using a helper-free triple transfection procedure and were purified by affinity chromatography (GE Healthcare). Viral titers were determined by quantitative PCR using Taq-Man technology (Life Technologies). The transfer plasmid was constructed by inserting a complementary DNA fragment and the WPRE sequence into an AAV backbone plasmid (pAAV-CMV, Stratagene).

AAV vector injection into fMRI-defined SI_{D2}

AAV vectors for neuron-specific expression of hM4Di and GFP were injected into SI_{D2}. AAV2.1-hSyn-hM4Di-IRES2-AcGFP ($3.8x10^{13}$ genome copy/ml) was for monkey 2, and a mixture of AAV2-CMV-hM4Di and AAV2-CMV-AcGFP ($1.9x10^{13}$ and $3.3x10^{13}$ genome copy/ml, respectively) for monkey 1. Note that both AAV2.1 (Kimura et al., 2021) and the combination of AAV2 and CMV promoter (Lerchner et al., 2014) have been reported to enable neuron-specific expression of target protein in macaques. Since the AAV vectors suitable for chemogenetic application have continuously been developed and improved by changing the serotype, promoter, and so on, we indeed selected the injected vectors that were considered the best available at the time of the injection to each animal. As a result, the AAV vectors used for individual animals differed, because monkeys 1 and 2 were subjected to vector injections separately at different time periods. The AAV vectors employed in these monkeys were indeed the same as those used in Nagai et al. (2016) and Nagai et al. (2020), respectively. To inject AAV vectors precisely into the functionally identified SI_{D2} (monkeys 1 and 2), we conducted fMRI-guided localization of injection sites as follows. For each monkey, we prepared a 3D plastic replica of the monkey brain of the same size as an actual brain made by using a 3D printer from data of a CT-scanned skull (acquired using Accuitomo170, J. MORITA CO., Kyoto, Japan), structural MRI, and fMRI activation map obtained by sensory stimulation of the contralateral hand D2 (Figure S1D, top). MR and CT images were overlaid using PMOD image analysis software (PMOD Technologies Ltd, Zurich, Switzerland). On the day of AAV vector injection surgery, the above replica brain was set to a stereotaxic instrument to obtain an approximate coordinate of the target of virus injections to cover the fMRI activation site using the same manipulator, injector, and syringe as those used in the subsequent actual injection (Figure S1D, top). The monkeys were initially anesthetized using ketamine (5-10 mg/kg) and xylazine (0.2-0.5 mg/kg), complemented with atropine, and the anesthesia was then maintained with approximately 1 to 2% isoflurane. Vital measures (heart rate, SpO_2, rectal temperature, and end-tidal CO_2) were continuously monitored throughout the surgery. Actual injection into the monkey brain (Figure S1D, bottom) was performed on the basis of the stereotaxic coordinate obtained using the replica with some fine (< 1 mm) tuning of the injection location during the surgery. Injections were conducted via a 10 μL syringe with a 33-gauge needle (NanoFil Syringe, MPI). The syringe was mounted into a motorized microinjector (Legato130, KD Scientific or UMP3T-2, WPI), which was held by a manipulator (model 1460, David Kopf) on the stereotaxic frame. After retracing the skin and galea, the parietal cortex was exposed by removing a bone flap and reflecting the dura matter. The injection needle was then inserted into the brain under an operating microscope (Leica M220, Leica Microsystems) and moved down 2.5 mm from the surface. The needle was then pulled up 0.5 mm, and the injection was started at 0.1 μl/min. Following each injection (1 μl), the needle was slowly pulled up following a 15-min wait to prevent backflow. In total, virus vector injections were conducted at four sites with an inter-site distance of approximately 1 to 1.5 mm, and their locations were set to cover the SI_{D2} identified by fMRI.

Histology and immunostaining

For histological inspection, monkeys were immobilized with ketamine (10 mg/kg, i.m.), and then deeply anesthetized with an overdose of sodium pentobarbital (80 mg/kg, i.v.) and transcardially perfused with saline at 4°C, followed by 4% paraformaldehyde in 0.1 M phosphate-buffered saline (PBS), pH 7.4. The brains were removed from the skull, postfixed in the same fresh fixative

overnight, saturated with 30% sucrose in phosphate buffer (PB) at 4°C, and then cut serially into 50-μm-thick sections on a freezing microtome. For visualization of immunoreactive signals of GFP, a series of every 6th section was immersed in 1% skim milk for 1 h at room temperature and incubated overnight at 4°C with rabbit anti-GFP monoclonal antibody (1:500; Thermo Fisher Scientific, MA, USA) in PBS containing 0.1% Triton X-100 and 1% normal goat serum for 2 days at 4°C. The sections were then incubated in the same fresh medium containing biotinylated goat anti-rabbit IgG antibody (1:1,000; Jackson ImmunoResearch, West Grove, PA, USA) for 2 h at room temperature, followed by avidin-biotin-peroxidase complex (ABC Elite, Vector Laboratories, Burlingame, CA, USA) for 1.5 h at room temperature. For visualization of the antigen, the sections were reacted in 0.05 M Tris-HCl buffer (pH 7.6) containing 0.04% diaminobenzidine (DAB), 0.04% $NiCl_2$, and 0.003% H_2O_2. The sections were mounted on gelatin-coated glass slides, air-dried, and coverslipped. A part of the other sections was Nissl-stained with 1% Cresyl violet. Images of sections were digitally captured using an optical microscope equipped with a high-grade charge-coupled device (CCD) camera (Biorevo, Keyence, Osaka, Japan).

In vivo PET visualization of DREADD expression

Before functional investigations of hM4Di, seven weeks following the virus injection surgery, the expression level and spatial distribution of the transduced hM4Di were first examined *in vivo* using PET with radio-labeled DREADD agonist ([^{11}C]DCZ) as tracer which specifically binds to the expressed DREADD (Nagai et al., 2020). PET scans were conducted using a microPET Focus 220 scanner (Siemens Medical Solutions USA, Malvern, USA). Anesthesia and vital monitoring were conducted as described above for the virus vector injection surgery. Transmission scans were performed for approximately 20 min with a Ge-68 source. Emission scans were acquired in 3D list mode with an energy window of 350–750 keV after intravenous bolus injection of [^{11}C]DCZ (344.8-369.6 MBq). Emission data acquisition lasted 90 min. PET images were reconstructed with filtered back-projection using a Hanning filter cut-off at a Nyquist frequency (0.5 mm^{-1}). To estimate the expression level of transduced DREADD *in vivo*, the specific binding of [^{11}C]DCZ was calculated as regional binding potential relative to nondisplaceable radioligand (BP_{ND}) using PMOD with an original multilinear reference tissue model (MRTMo) (Nagai et al., 2020). Since the signal in the BP_{ND} image of [^{11}C]DCZ reflects both DREADD expression and background tracer binding (i.e., noise) (Yan et al., 2021), we removed the background noise by subtracting the BP_{ND} value obtained with the control data of the same individual in which DREADD was not expressed (Oyama et al., 2021). The control data was obtained before AAV injection for monkey 2. Due to the lack of data of before AAV injection in monkey 1, signals in the BP_{ND} image of monkey 1 in the right and left hemispheres were flipped to each other to create the control image which does not contain the signal reflecting DREADD expression in the AAV-injected hemisphere. Both the original and control data of monkey 1 was then spatially normalized to the template structural MR image (McLaren et al., 2009) to calculate the background-subtracted BP_{ND} image, which was finally inverse transformed to the original image space. The resultant subtracted BP_{ND} images of both monkeys were spatially smoothed with an isotropic Gaussian kernel (full width at half maximum, 3 mm).

Behavioral tests

Manual dexterity of monkeys expressing hM4Di in SI_{D2} was tested using a modified Brinkman board task (Brinkman and Kuypers, 1973; Rouiller et al., 1998) as follows. A plastic board with 20 rectangular slots (5 × 10 mm with 5-mm depth for each) was placed in front of a monkey chair. Monkeys picked up a small object (a piece of chocolate flake, approximate diameter 4 mm) from each slot. Monkeys consistently used their thumb and index fingers to pick up the object (i.e., precision grip) (Nishimura et al., 2007; Sawada et al., 2015; Brinkman, 1984) (Figure 2A). In each trial, monkeys picked up objects from ten slots in total with either contralateral or ipsilateral hand to the hM4Di-expressing hemisphere, and the amount of time needed to pick up all the ten objects was measured. The time to complete each trial was normalized with the number of objects correctly picked up to obtain the value that reflected the manual dexterity. In a single experimental session, monkeys performed five to ten trials with each of contralateral or ipsilateral hand both before and after intravenous systemic administration of DCZ (MedChemExpress) at the same dose as that used for behavioral experiments with hM4Di in previous studies (0.1 mg/kg) (Nagai et al., 2020; Oyama et al., 2021). The behavioral test in the DCZ condition began 10 min after the administration. To examine the effect of DCZ on hand reaching, we also conducted a control task for monkey 2, in which the time consumed for more course grasping of larger objects (with whole hand) placed on a flat plate without slots was measured. This task included similar hand reaching as that in the modified Brinkman board task described above, but manual dexterity was only minimally required. The amount of time required to pick up five pieces of a large object (square-shaped sweet potato with 15 × 15 × 15 mm in size for each) using the hand contralateral to the hM4Di-expressing SI was measured, and normalized with the number of correctly picked up objects. Five to ten trials were conducted both before and after intravenous systemic administration of DCZ (0.1 mg/kg). The time interval between the administration and trial restart was the same as that for the Brinkman board task described above.

Sensitivity to cold stimulation applied to the foot sole was tested in monkeys 2 and 3. The monkeys were trained to place the foot sole on a metal plate in front of a monkey chair. The surface temperature of the plate could be manipulated with the precision of 0.1°C (Cool Plate SCP-85, AS ONE). The monkeys' foot withdrawal from the plate was not physically restricted. The foot withdrawal latency from the plate was measured as an index of sensitivity to a cutaneous (cold) stimulus. If the monkey did not withdraw the foot within 60 s, the trial was terminated and the withdraw latency of 60 s was assigned for that trial. The monkeys performed five to ten trials for each of two temperature conditions (30°C for control and 10°C for cold stimulation) both before and after intravenous administration

of DCZ (0.1 mg/kg). The time interval between the administration and trial restart was the same as that for the modified Brinkman board task described above.

MRI scanning

Monkeys were first lightly sedated with ketamine (5-10 mg/kg), complemented with xylazine (0.2-0.5 mg/kg), and then transferred to a 7T MRI scanner (Magnet: KOBELCO/JASTEC, Japan; Spectrometer and console: AVANCE-I, Bruker Biospin, Ettlingen, Germany) from their home cage. Each monkey was then placed into the scanner with a bore diameter of 40 cm, in which the head was immobilized. A 20-cm inner-diameter volume resonator (Takashima, Tokyo, Japan) was used for transmission. In the scanner, the monkey was maintained under light sedation with propofol (0.2-0.6 mg/kg) throughout the scanning session while continuously being monitored for SPO_2, heart rate, and rectal temperature (FOT-M and FTI-10, FISO Technologies, Quebec, Canada and E5CN, Omron, Kyoto, Japan). Following the setup, functional images were acquired via gradient-echo echo-planer imaging (EPI) sequence using a 4-ch phased array receiver coil (Rapid Biomedical, Rimpar, Germany) with the following scan parameters: repetition time (TR), 4 s; 4-shot; echo time (TE), 15 ms; flip angle, 60°; field of view (FOV), 120 × 120 mm; matrix size, 64 × 64; slice thickness, 1.1 mm; no spatial gap between slices; 23 horizontal slices (Figures S1A and S1B). BOLD signal in response to cutaneous tactile stimulation was obtained with a block-design fMRI (Chen et al., 2007; Cléry et al., 2020; Dutta et al., 2014; Hayashi et al., 1999; Lipton et al., 2006; Nagasaka et al., 2020; Sharma et al., 2018; Wang et al., 2013; Yang et al., 2021). All EPIs for the following analyses were obtained at least 1 h following the ketamine administration to minimize its influence on the BOLD signal intensity. A scanning run began with a 2-min blank period before starting the first stimulation block for both stabilization of the MR signal and the preparation for stimulation. In the scanner, gentle cutaneous stimulation was manually applied to the index finger (D2) of either right or left hand of the monkey for 1 min using a small brush with a stroke frequency of approximately 4 Hz. The stimulation block was then followed by a 1-min rest period without stimulation (baseline) and subsequent stimulation of the opposite hand in the same manner (Figure S1C). A scanning run was ended after four cycles of stimulation and rest blocks for both hands, and as a result, the total time of a single run was 18 minutes (2 + 4 × 4 minutes, 270 volumes). A single scanning session was composed of five to six runs in total. Prior to functional scans, structural image of the monkey brain was obtained using a fast low-angle shot (FLASH) sequence (Frahm et al., 1986) with the same slice configuration and spatial resolution as that for obtaining EPIs. High-resolution structural image of the whole brain was separately acquired for the same animal using the FLASH sequence with the following scan parameters: TR, 660 ms; TE, 13.37 ms; flip angle, 20°; FOV, 150 × 150 mm; matrix size, 512 × 512; slice thickness, 1 mm; no spatial gap between slices; four sets of 24 coronal slices covering the whole brain. A scanning session with vehicle [2% dimethyl sulfoxide (DMSO) in a total 1 mL saline, without DCZ] administration was followed by the next session with DCZ administration with a session-to-session interval of at least two weeks for recovery from anesthesia, which was then followed by the next cycle of vehicle and DCZ sessions. In total, EPIs during hand D2 stimulation in monkey 1 were acquired in eight scanning sessions including 17 and 20 runs for vehicle and DCZ condition, respectively (four sessions each). EPIs during hand D2 stimulation in monkey 2 were acquired in six scanning sessions including 17 and 18 runs for vehicle and DCZ condition, respectively (three sessions each). Similarly, EPIs during foot sole stimulation in monkey 1 were acquired in two sessions including five runs for both vehicle and DCZ conditions. EPIs with foot sole stimulation in monkey 2 were acquired in four sessions including 11 and 10 runs for vehicle and DCZ condition, respectively (two sessions each). DCZ (0.1 mg/kg) or its corresponding vehicle was systemically injected intravenously 10 min before the first run of the session. A single scanning session without vehicle or DCZ administration was conducted before the virus vector injection to functionally localize SI activation in response to cutaneous tactile stimulation of the contralateral hand D2.

MRI data analyses

MRI data analyses were conducted using statistical parametrical mapping (SPM12) software on MATLAB (MathWorks). EPIs obtained during the blank period in each run were not included in the following analyses. Functional images obtained across different scanning runs for each animal were realigned and unwarped for correcting for magnetic field inhomogeneities due to animal motion (minimal due to anesthesia, if any), and they were coregistered to the structural image of the same monkey. The resultant functional images were further coregistered to the high-resolution structural image of the whole brain obtained from the same animal. The functional images were then spatially smoothed with an isotropic Gaussian kernel (full width at half maximum, 3 mm). Data were high-pass filtered with a cut-off of 480 s for detrending. Brain activation for cutaneous stimulation was then calculated for each condition for each animal as the contrast between the BOLD signals obtained during stimulation and rest blocks via voxel-wise general linear model analysis with default hemodynamic response function implemented in SPM 12. Activity difference between vehicle and DCZ conditions was calculated as the condition-dependent difference in the contrast between stimulation and baseline (Nagasaka et al., 2017). The threshold for statistical significance was set at $p < 0.05$ familywise error (FWE) corrected for multiple comparisons or $p < 0.001$ uncorrected. For ROI analysis of sensory-evoked BOLD signal, percent signal change from baseline was calculated for each functional ROI for each scanning run using MarsBaR region of interest toolbox for SPM (Cléry et al., 2020; Nelissen et al., 2011; Nelissen and Vanduffel, 2011; Sani et al., 2021; Sharma et al., 2018). Functional ROI in SI_{D2} was calculated using thresholded ($p < 0.05$, FWE-corrected) SPM *t*-maps obtained for control (vehicle) condition, as continuous voxels within a 2-mm radius centered at the local maximum (Bogadhi et al., 2019). Functional ROIs for the hand region in areas 5, 7, and SII were calculated using thresholded ($p < 0.001$, uncorrected) *t*-maps obtained for the

contrast between vehicle and DCZ conditions (see above) as all voxels within the corresponding clusters (i.e., clusters in areas 5, 7, and SII), and the ROIs for the foot region in SI and SII were calculated using the thresholded ($p < 0.001$, uncorrected) *t*-map obtained in the DCZ condition as all voxels within the corresponding clusters (SI and SII). Psycho-physiological interaction (PPI) analysis (Friston et al., 1997) was conducted using SPM12 with the functional ROI in the SI_{D2} described above as a seed region to examine the functional connectivity with SI_{D2} during sensory stimulation of the contralateral hand D2. The activity of remote brain regions was regressed on a voxel-wise basis against the product of time series of the seed region and the vector of the psychological variable of interest (hand stimulation contralateral to the DREADD-expressing hemisphere minus baseline), while the physiological and the psychological variables themselves were included as regressors of no interest. Statistical threshold was set at $p < 0.05$, FWE-corrected.

Neuron, Volume *109*

Supplemental information

Chemogenetic sensory fMRI reveals behaviorally relevant bidirectional changes in primate somatosensory network

Toshiyuki Hirabayashi, Yuji Nagai, Yukiko Hori, Ken-ichi Inoue, Ichio Aoki, Masahiko Takada, Tetsuya Suhara, Makoto Higuchi, and Takafumi Minamimoto

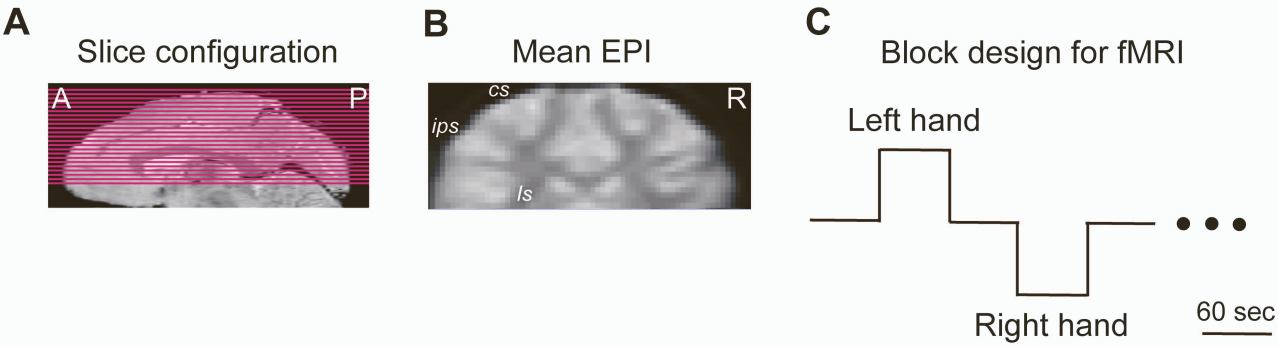

Fig. S1

Figure S1. Experimental design of fMRI and fMRI-guided DREADD transduction. Related to Figure 1.

(A) Slice configuration (magenta) for fMRI overlaid on a sagittal slice of whole brain structural MRI (see STAR Methods). A, anterior; P, posterior. **(B)** A reconstructed coronal section of the mean EPI across sessions acquired from monkey 1 receiving tactile stimulation of hand D2. R, right; cs, central sulcus; ips, intraparietal sulcus; ls, lateral sulcus. **(C)** Block design for fMRI. Left hand and Right hand, stimulation period of the left and right hand, respectively. **(D)** MRI/CT fusion-based precise localization of viral vector injection sites for DREADD expression at SI_{D2} (see STAR Methods). Top, 3D model brain of monkey 1 attached to a stereo apparatus. The model was made by 3D printer based on the spatially aligned structural MRI (gray) and CT (white) data of the brain and skull with coregistered activation map (white arrow, black circle just posterior to the central sulcus) obtained via fMRI with contralateral hand D2 stimulation prior to the viral vector injection. Although the sulcal information was reflected on the model brain, major sulci of the brain were exaggerated by post-hoc marking (blue) to aid visualization. Stereo coordinates of injection sites were determined based on the location of the activation site on the model brain. Bottom, actual viral vector injection into the brain of monkey 1. Injection coordinates were further refined following attachment of the monkey to the stereo, based on the location of the central sulcus as a major landmark. **(E)** BOLD response in the contralateral SI to the cutaneous tactile stimulation of hand D2 (top) and the [^{11}C]DCZ PET image showing DREADD expression (bottom) in monkey 2. **(F)** [^{11}C]DCZ-PET images showing DREADD expression across the whole brain in monkey 1 (top) and monkey 2 (bottom). Inter-image interval, 2 mm. In both monkeys, DREADD expression was specifically observed in the SI_{D2}, where the DREADD-encoding AAV was injected.

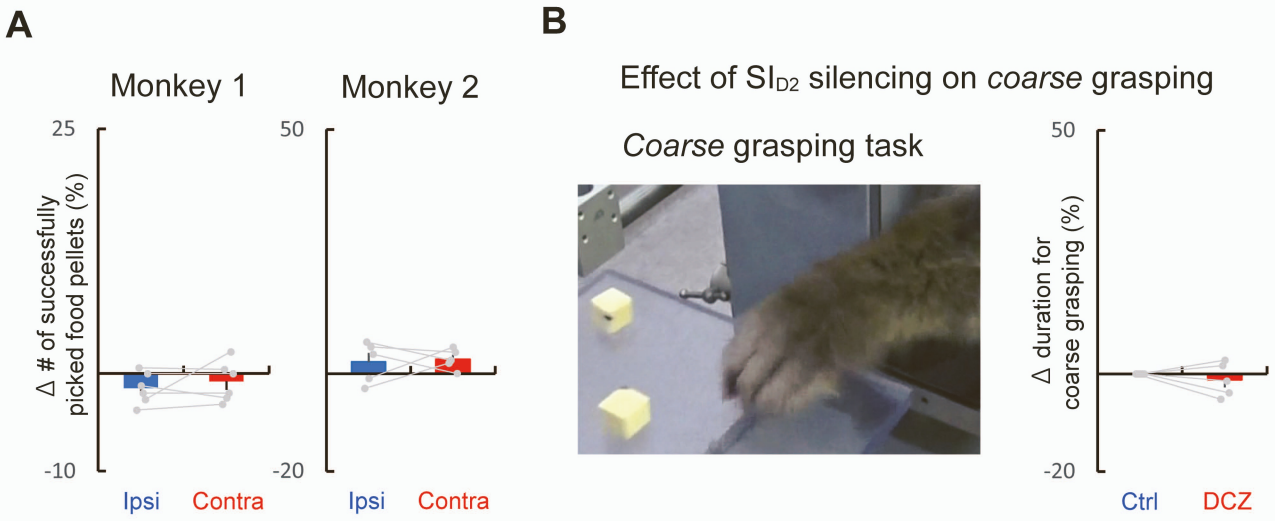

Fig. S2

Figure S2. DREADD-induced silencing of SI_{D2} did not affect the number of correctly picked objects in the fine grasping task or the performance of the coarse grasping task. Related to Figure 2.

(A) DCZ-induced change in the number of correctly picked objects in the fine grasping task. Negative value represents decrease in the correctly picked objects following DCZ administration. Gray line depicts the performance in each session. Error bars, s.e.m. DCZ administration did not significantly affect the number of correctly picked objects for either ipsilateral or contralateral hand condition in either monkey. **(B)** Course grasping of large objects with whole hand contralateral to the DREADD-expressing SI_{D2} (left) and performance of the course grasping task for monkey 2 (right). Positive value represents delayed performance following DCZ administration. Gray line depicts the performance in each session. Error bars, s.e.m. In contrast to the fine grasping task, no significant change was observed in the performance following DCZ administration.

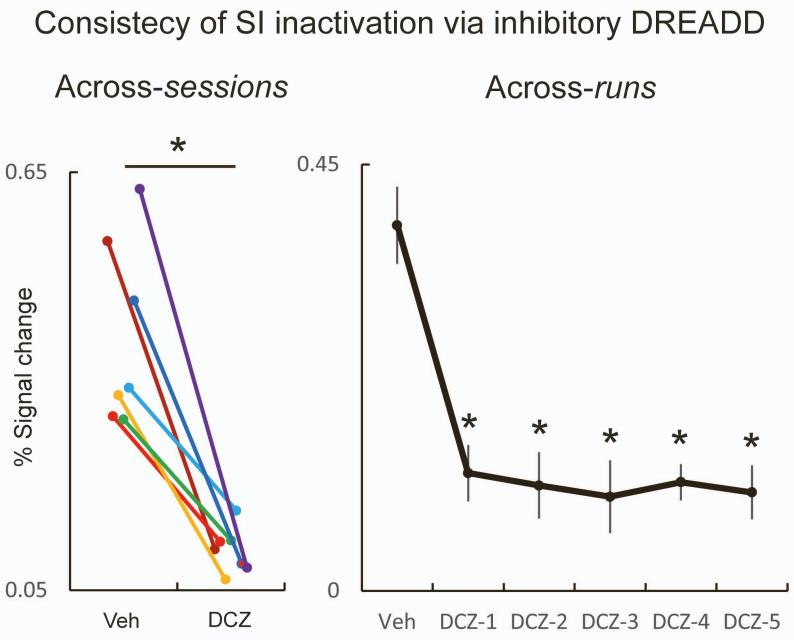

Fig. S3

Figure S3. Consistency of DREADD-induced SI_{D2} silencing across different scanning *sessions* and *runs*. Related to Figure 3.

Left, consistency of DREADD-induced SI_{D2} silencing across different scanning *sessions*. Data points linked by line depict the percent signal change in SI_{D2} induced by the stimulation of the contralateral hand D2 for a pair of sequential sessions in vehicle and DCZ conditions. *: $P < 0.02$, paired *t*-test. n = 7 pairs of sessions (four and three pairs for Monkeys 1 and 2, respectively). Note that signal reduction in DCZ condition compared to vehicle control condition was observed for all the pairs of sequential sessions without exception, indicating reliable and consistent silencing across different sessions. Right, consistency of DREADD-induced SI inactivation across different scanning *runs* within a given session. Error bars, s.e.m. * indicates significant ($P < 0.03$, unpaired *t*-test, corrected for multiple comparisons) difference between vehicle and DCZ conditions. DCZ-induced signal reduction compared to vehicle control condition was consistent across different scanning runs, suggesting both rapid and stable effect of DCZ within a given session (Nagai et al., 2020).

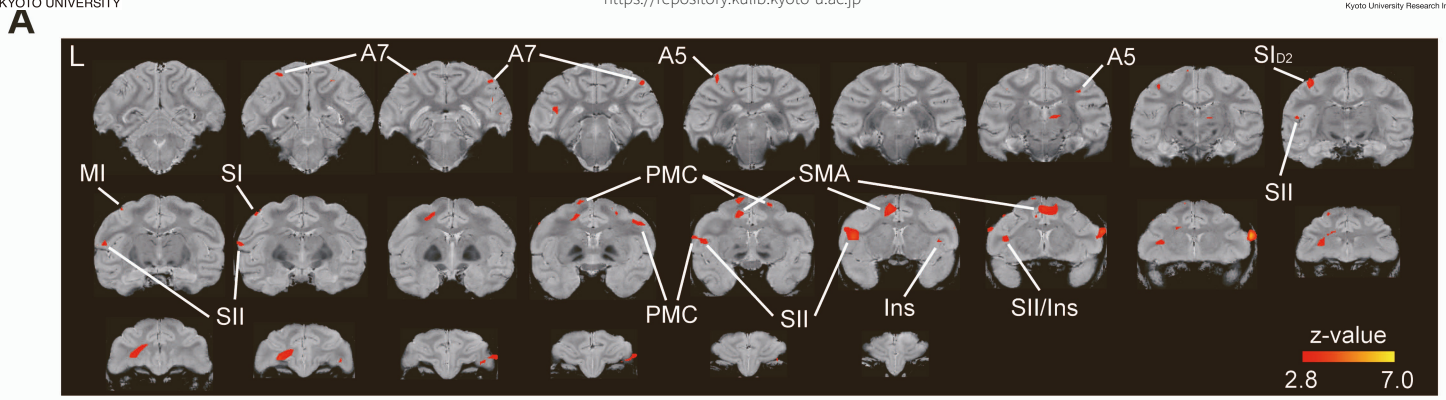

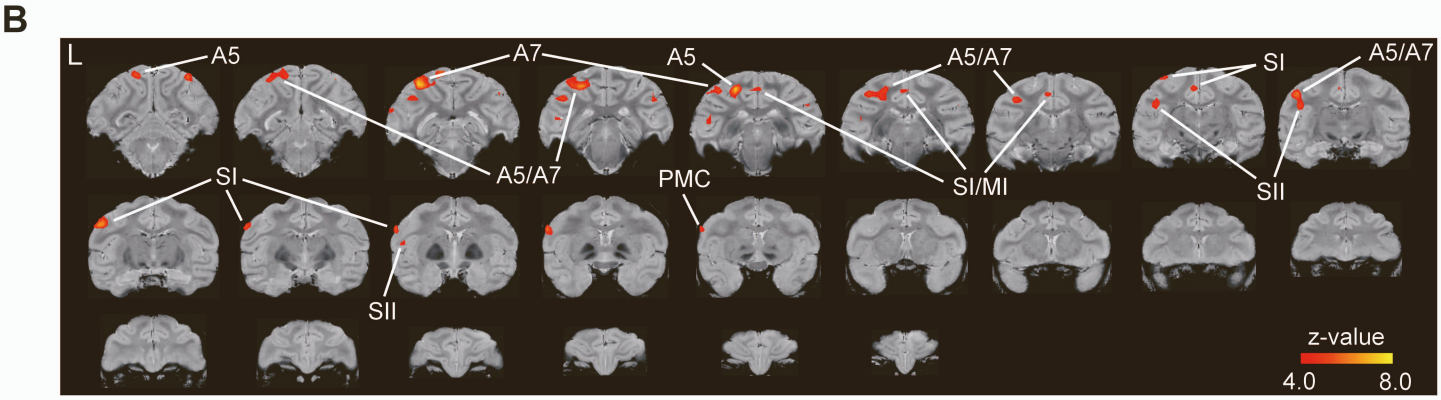

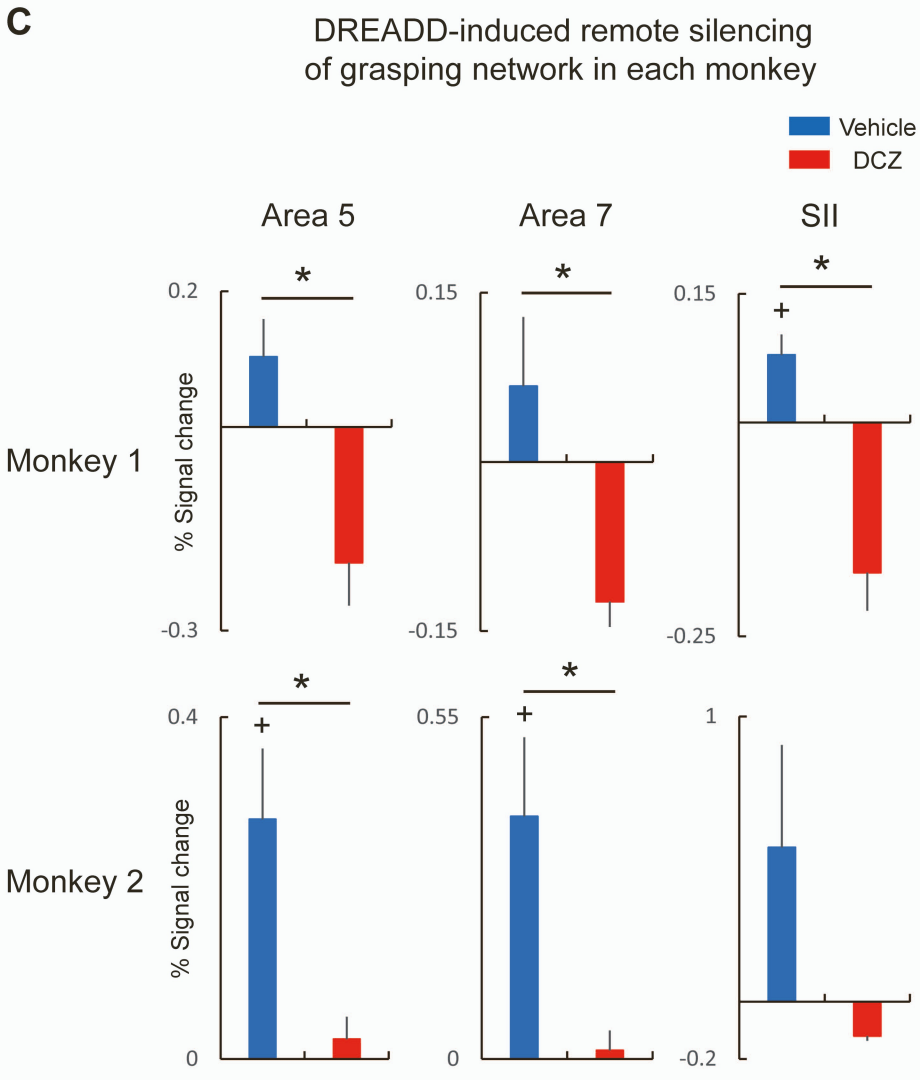

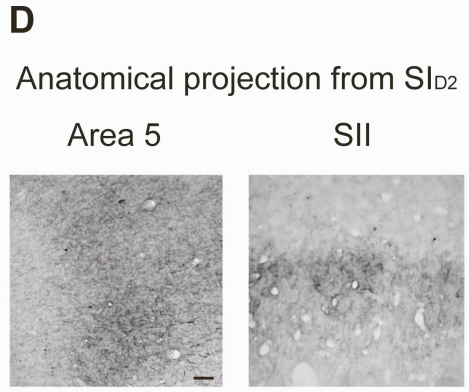

Fig. S4

Figure S4. DREADD-induced attenuation of sensory-evoked BOLD responses in remote areas of grasping-related network. Related to Figure 4.

(A and B) Whole-brain analysis of the DCZ-induced attenuation of the sensory-evoked BOLD response (A) and the functional connectivity (PPI) with DREADD-expressing SI_{D2} in the vehicle condition (B) for the same monkey as in Figure 4. Inter-image interval, 2 mm. L, left. In addition to the three areas depicted in Figure 4, this analysis showed significant signal attenuation in several other remote areas including the primary motor cortex (MI), the premotor cortex (PMC), and the supplementary motor area (SMA) ($P < 0.001$, uncorrected), all of which are known to be involved in the grasping behavior (Borra et al., 2017; Brinkman, 1984; Brochier et al., 1999; Castiello, 2005; Davare et al., 2011; Fogassi et al., 2001; Gerbella et al., 2017; Jeannerod et al., 1995; Lega et al., 2020; Nelissen and Vanduffel, 2011; Rizzolatti and Luppino, 2001; Sharma et al., 2018). **(C)** DREADD-induced modulation of BOLD response in area 5 (left), area 7 (middle), and SII (right) for each monkey. Error bars, s.e.m. *: $P < 0.03$, unpaired *t*-test, corrected for multiple comparisons. +: $P < 0.03$, paired *t*-test for difference from the baseline, corrected for multiple comparisons. Note that the response below the baseline was observed in the DCZ condition in monkey 1 specifically at remote regions (areas 5, 7, and SII), but not at the DREADD expressing SI_{D2}, suggesting that it is not the result of non-specific effect including general baseline increase across the whole brain. But instead, it might be the reflection of complex network operation as a result of SI_{D2} silencing. Since the response below the baseline was observed only in one of the two monkeys tested, its interpretation would be rather limited. **(D)** Magnified images of axon terminals of SI_{D2} neurons expressing the co-transduced GFP in area 5 (left) and SII (right) in monkey 1, depicting anatomical projection from DREADD-expressing SI_{D2}. Scale bar, 100 μm.

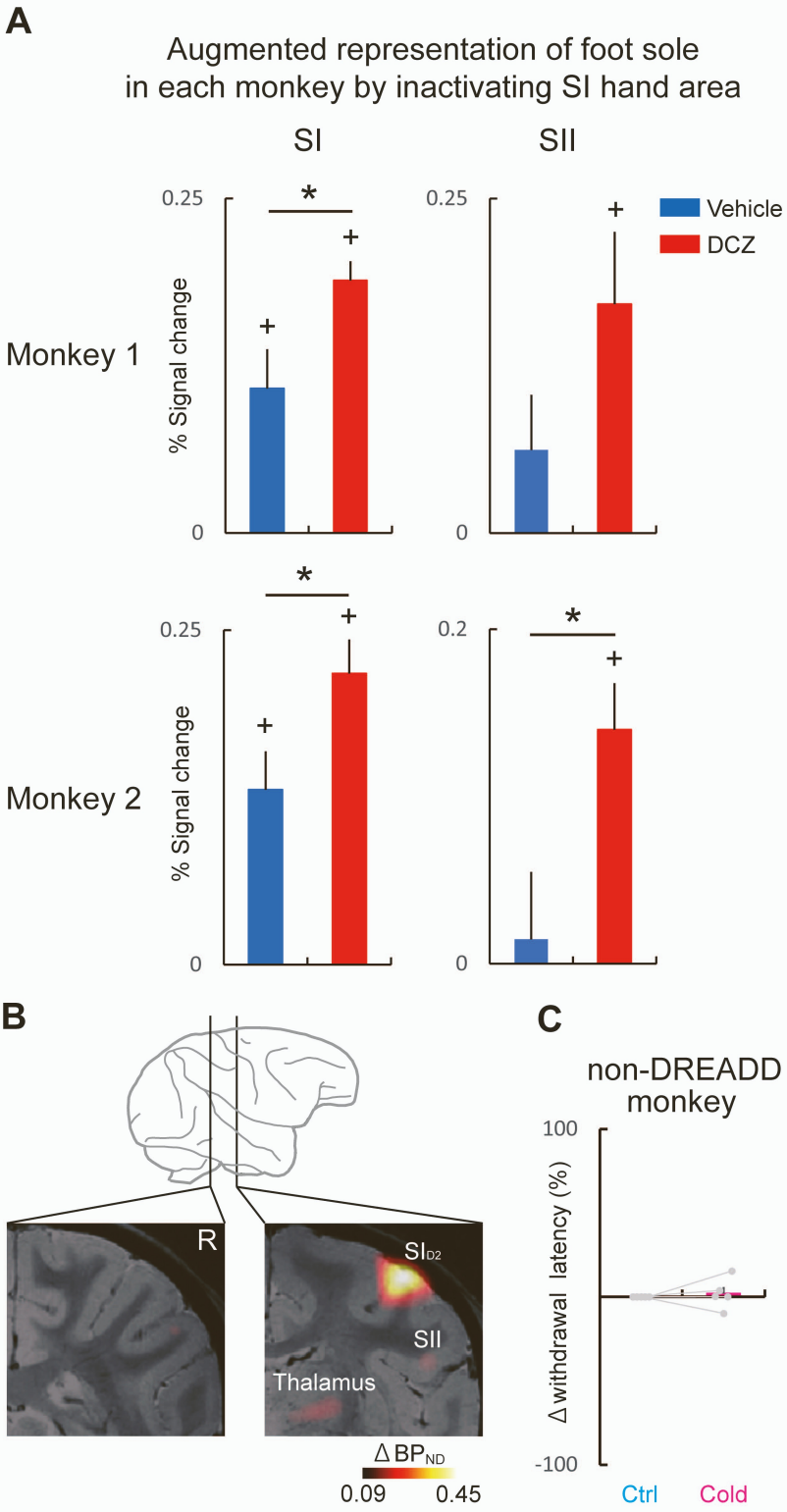

Fig. S5

Figure S5. Upregulation of foot sole representation induced by focal silencing of SI_{D2} in each monkey. Related to Figure 5.

(A) Augmentation of foot sole representation in SI (left) and SII (right) for each monkey induced by focal silencing of SI_{D2}. Error bars, s.e.m. *: $P < 0.04$, unpaired *t*-test. +: $P < 0.02$, paired *t*-test for difference from baseline. **(B)** PET analysis in monkey 2 showed that DREADD expression could not be detected within the SI foot sole region even at a lower threshold (left), where DREADD in the axon terminal of SI_{D2} neurons was observed (Nagai et al., 2020; Oyama et al., 2021) in the SII and the thalamus (right). R, right. This result was histologically confirmed as well (data not shown). Note that the threshold was lower than the value required for noise removal. **(C)** DCZ-induced change in the withdrawal latency of the foot sole from cold (magenta) or control (cyan) stimulation in a naïve control monkey without DREADD expression (monkey 3). Negative value represents shortened withdrawal latency following DCZ administration. Gray line depicts the performance in each session. Error bars, s.e.m.